Improved Nuclear SIte characterization for waste minimization in DD operations under constrained EnviRonment

Research and Innovation action
NFRP-2016-2017-1

WP3 –Sampling strategy Statistical guideline

Deliverable 3.7

Appendix 2: UC2

Version n° 1

Authors: Bart Rogiers, Wouter Broeckx , Sven Boden (SCK CEN)

http://www.insider-h2020.eu

Document Information

Grant Agreement #:	755554
Project Title:	Improved Nuclear SIte characterization for waste minimization in DD operations under constrained EnviRonment
Project Acronym:	INSIDER
Project Start Date:	01 June 2017
Related work package:	WP 3: Sampling strategy
Lead Organisation:	SCK CEN
Submission date:	2018-01-31
Dissemination Level:	CO

History

Date	Submitted by	Reviewed by	Version (Notes)
2021-10-26	Sven Boden	Bart Rogiers Wouter Broeckx	1.0

Contents

Abbreviations

BR3	Belgian Reactor number 3
NST	Neutron Shield Tank
SCK CEN	Belgian Nuclear Research Centre
UC	Use Case

This annex describes the data analysis and sampling design strategy implementation for the initial radiological characterisation of the **biological shield of the Belgian Reactor 3 (Use Case 2)**. The first chapter introduces the use case and the **overall strategy implementation classified in three implementation stages**. Chapter 2 describes the sampling plan development starting from the data analysis of the pre-existing data, further identified as stage 1. Stage 2 consists of the execution of the sampling plan followed by the data analysis on the combined dataset (pre-existing and new data) and is outlined in chapter 3. Chapter 4 explains the third and final stage, consisting of additional data gathering and the final data analysis on the entire dataset. The variety of supplementary quality control measurements performed is described in Chapter 5 and the lessons learnt are summarized in Chapter 6.

1 Case introduction & overall strategy implementation

This chapter briefly introduces the use case, summarizes its objectives and constraints and describes the three implementation stages of the overall INSIDER data analysis and sampling design strategy for UC2. More details regarding the case introduction and the first stage are available in (Boden, 2018) as well as (Broeckx, et al., 2020).

1.1 Case introduction

BR3 was a relatively small 10 MWe (about 41 MWth) pressurised water reactor of the SCK CEN (Belgian Nuclear Research Centre). It acted as a pilot reactor for the later nuclear commercial power plants in Belgium, was brought into operation in October 1962 and was shut down in 1987 after 25 years of operation and eleven campaigns. Figure 1 shows a cross section of the reactor building during exploitation. The entire primary circuit (reactor pressure vessel, steam generator, pumps & primary loop, *etc.*) has been dismantled, as well as the ventilation and the anti-missile slabs. The bottom part of the reactor building consists of reinforced ordinary concrete. The remainder of the reactor building consists of reinforced heavy concrete. The concrete of the reactor pool close to the reactor pressure vessel is activated. Since the reactor pressure vessel was surrounded by a neutron shield tank (NST), the surrounding concrete is not activated, except locally near the hot and cold legs. In a first, very rough estimation based on a limited amount of exploratory historical measurements, the activated part of the concrete is marked in red colour.

Based on extensive and more accurate 3D modelling of the geometry of the different components and concrete elements, the 3D scene in Figure 2a was constructed that served as a geometrical/positional reference during this study. Figure 2b includes the distribution of two different types of reinforced heavy concrete, to the best of our knowledge, which will have an impact on the estimated activation levels (see Section 4.2 for more details).

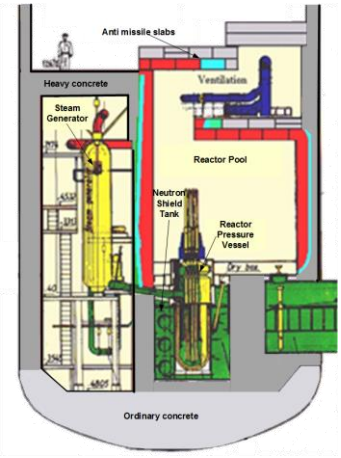

Figure 1: Cross section of the BR3 reactor building during exploitation showing the main components. The building structure is mainly composed of reinforced ordinary concrete (bottom plate) and reinforced heavy concrete (upper structure). The activated concrete is marked in red colour (first rough estimation).

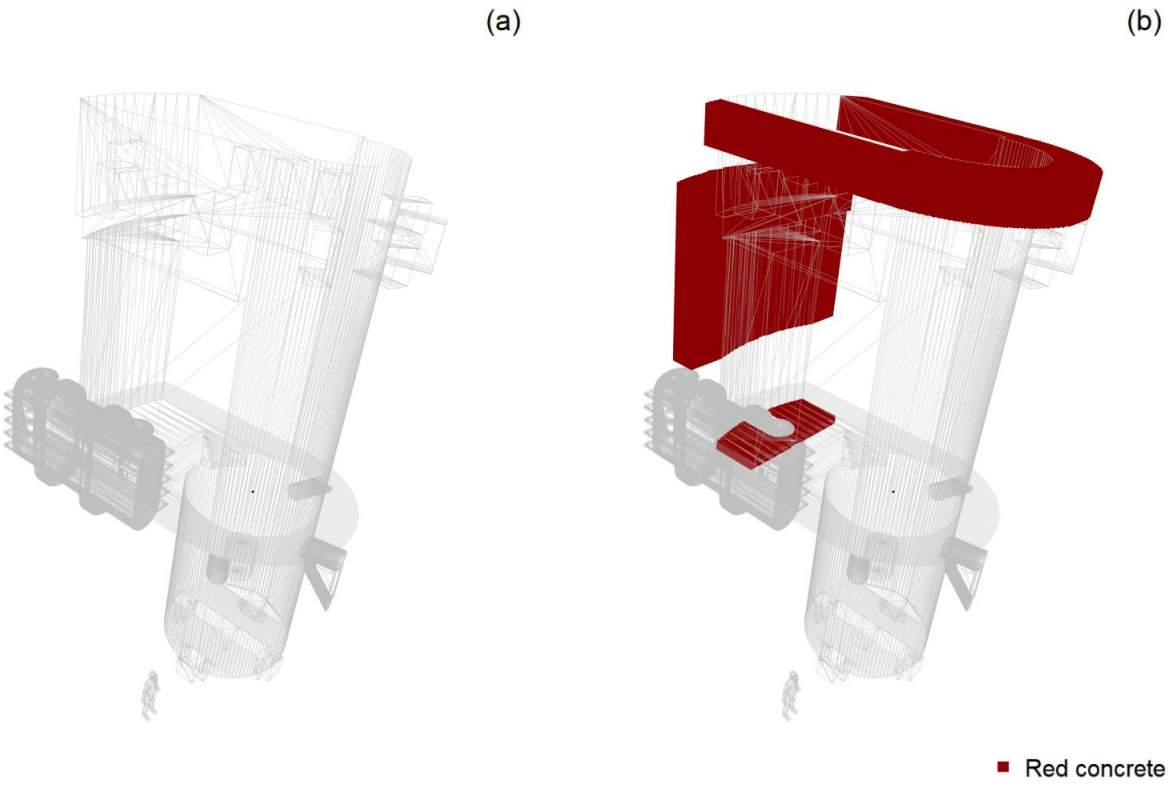

Figure 2: A 3D scene (a) including the inner surface of the wall, the hot and cold legs, and fuel transfer tank geometries, which is used as reference for some illustrative 3D views throughout the document. The presence of concrete of the "red" type (see also Secion 4.2) is indicated in (b). Note these 2D displays of 3D scenes prohibit very exact interpretation of the geometry and data locations, but given the strong 3D nature of this use case, we do not really see any other way to provide a concise overview in a static document like this.

1.2 Objectives

The SCK CEN developed a radiological characterization program aiming at economically optimizing the biological shield dismantling strategy using a waste-led approach. In order to reach this **main goal,** three **objectives** were formulated:

1. Create a sufficiently reliable 3D activity concentration distribution model, that includes uncertainty estimates.
2. Economically optimise volumes in view of a waste-led approach taking the following end stage options into account:
   - unconditional release, and
   - conditional release.
3. Quantify and localise the different end-stage volumes.

For the "sufficient reliability" of the 3D activity concentration distribution model, we mainly looked at the following **sub-objectives**:

1.A. The model results should include as much as possible the known anomalies in the 3D activation,
1.B. The model results should not be in conflict with the (potentially revised) expectations of the experts involved,
1.C. The data used should at least cover bottom to top of all sides of the biological shield, in order to avoid extrapolation as much as possible, and be of sufficient quality,
1.D. In case any of the above elements are violated, good arguments should be available to deviate locally from the model results,
1.E. The model results should be validated/tested, especially in case very flexible non-linear types of methods are used, to avoid overfitting.

For the determination and localization of the two end-stage volumes, the following thresholds (activity concentration levels in Bq/g) should be applied:

- $\text{Unconditional release: } \left(\frac{\text{Ba133}}{0.1} + \frac{\text{Eu152}}{0.1} + \frac{\text{Co60}}{0.1}\right) < 1$
- $\text{Conditional release: } \left(\frac{\text{Ba133}}{0.1} + \frac{\text{Eu152}}{0.1} + \frac{\text{Co60}}{0.1}\right) \geq 1$

We furthermore worked with the following assumptions:

- The probability to exceed the threshold should be less than 5%, for demonstrating compliance with the threshold; and
- The threshold value can also be considered as an average value for a mass of 1 ton. For the BR3 biological shield (density concrete of 3.5 g /cm³), this means that we can average over cubes of 0.66 x 0.66 x 0.66 m³, if this might economically optimise the end stage volumes.

In view of performing a dose impact study for the conditional release, it was required to know the total activity (50th and 95th percentile) and the activity concentrations (50th and 95th percentile).

1.3 Constraints

Nuclear safety **constraints** were rather limited, taking into account that the expected activation levels were relatively low. Most important constraints are related to accessibility limitations and

therefore classical safety issues. Furthermore, there are always economical limitations (number of samples) and sampling was hampered by the presence of thick reinforcement bars.

1.4 Gather pre-existing data

We had the following **pre-existing data** at our disposal (Boden, 2018):

- Original 2D plans and 3D geometric models based on the original 2D plans (not “as-built”);
- Operational history;
- Results from neutron activation calculations; and
- Results from radiological measurements whether or not connected to BR3 dismantling activities:
    - Removal of anti-missile slabs (1994).
    - Bioshield sampling programme 1, also indicated as “Mandoki” (1996).
    - Creation of an opening for the decontamination of the steam generator, also indicated as “Block 10” (2001).
    - Bioshield sampling programme 2, also indicated as “Piccini” (2008).
    - Removal of the hot leg, also indicated as “Hot-leg” (primary loop, 2012).
    - Inspection of the bottom of the reactor/NST pit (2016).
    - Removal of the pool liner (2018), also indicated as “Liner”.

Based on the analysis of the results from pre-existing data, we concluded that for the end-stages of unconditional release and conditional release the only **radionuclides to be taken into account** were:

- Co-60, Ba-133, Eu-152 for the activated concrete.
- Co-60 for the reinforcement bars (only from the year 2027 on Ni-63 should be taken into account as well).

Moreover, the Co-60 concentration in the reinforcement bars is about 5 times lower than the Ba-133 concentration in the concrete at the same location on the reference date (1 January 2020). This means that, when the Ba-133 concentration would be below the clearance level in the concrete at a specific location, this will be the case for the Co-60 in the reinforcement bars as well, at the same location. Hence, in this study, we do not differentiate the reinforcement bars from the concrete.

1.5 Is data sufficient for analysis

The diverse existing dataset was being considered as sufficiently large and adequate for performing a first data analysis in order to guide further sampling.

1.6 Various stages implementing the overall strategy

Referring to the data analysis and sampling design strategy developed within the INSIDER project, we categorized the overall strategy implementation in three stages:

- Stage 1 (Section 2): Preliminary data analysis based on pre-existing data followed by sampling design since this was not sufficient to achieve the objectives, especially 1.C was not met at this stage, which lead to a limited analysis also not targeting *e.g.* 1.A and 1.E.
- Stage 2 (Section 3).: Execution of the first sampling plan and corresponding data analysis, followed by additional sampling design since the objectives were still not fully achieved (especially 1.A and 1.C)
- Stage 3 (Section 4): Additional data gathering followed by the final data analysis on the full dataset, after which the data and model were considered sufficiently adequate for meeting the objectives.

An overview of all data available after stage 3 is provided in Table 1, and presented Figure 3. We will further detail in the next three sections which data was available at the start, was gathered during, and was omitted from the analysis in the corresponding investigation stages.

Table 1: Summary of the available date in the various stages

Data type	Stage 1 Pre-existing	Stage 2 Gathered during INSIDER project	Stage 3 Additional gathered during INSIDER project
Borehole	Block-10 Hot-leg Mandoki Piccini	Insider	Insider
Other	Liner	Como-18	Como-19 Insider

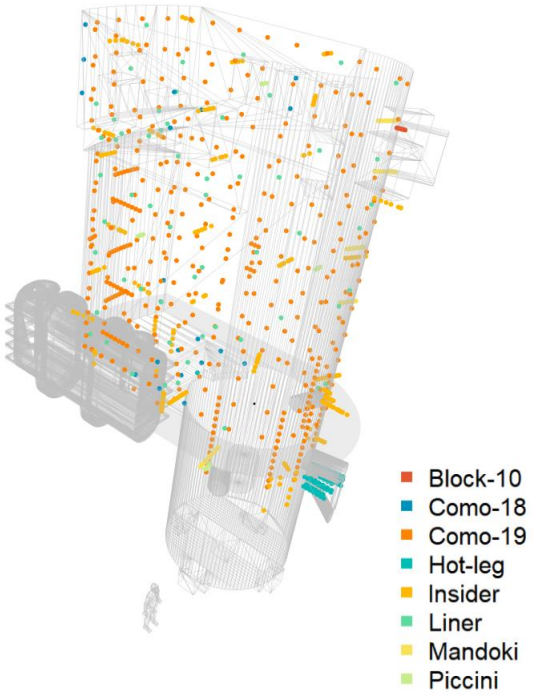

Figure 3: Overview of all data points available after stage 3, with an indication of the different data collection campaigns. For more details, see Sections 2 to 4.

2 Stage 1: Preliminary data analysis based on pre-existing data & sampling design

In view of achieving the main goal, we applied the INSIDER data analysis and sampling design strategy by pre-processing the existing data, performing the exploratory data analysis followed by the actual data analysis. We used the obtained results to develop the sampling design for stage 2.

2.1 Pre-processing

The pre-processing of the data basically consisted of three different aspects:

1. The 3D location of the different measurements was not directly recorded, and had to be inferred based on the 3D geometric model of the biological shield, and the recorded positions in terms of 2D coordinates for the specific concrete elements (see *e.g.* the wall IDs in Figure 5), the angles of the boreholes and the depth of the samples with respect to the inner or outer surface of the biological shield. As this is not straightforward given the complexity of the 3D geometry of the biological shield, it required different iterations between the 3D geometric model and data analysis experts. Both the liner and borehole sample locations available at this stage are shown in Figure 4.
2. The 3D geometry of the biological shield itself had to be converted into an effective format that would allow efficient estimation of the activity concentrations across the entire volume. We opted for using regular grids, with point locations separated by a constant distance d in x, y as well as z directions. In this way, estimates could be made on a point-by-point basis, and every point is approximately representative for a volume of d^3. To reconstruct the volume, we made use of different base maps (*i.e.* horizontal slices through different parts of the bioshield) like those included in Figure 5. For the more complex geometries, the existing 3D meshes were used directly for subsetting the regular grids (see *e.g.* cilinders corresponding to the hot and cold legs in Figure 2a). The origin of the unified 3D coordinate system used for this purpose was put in the center of the NST pit, at its top, which corresponds to the level of the reactor pool bottom (see the origin in Figure 5 and the corresponding black point in Figure 2a). We provide an overview of the different obtained grids in Figure 6. The coarser grids were used for model development, prototyping and testing purposes, while the final calculations were performed for the 10 cm spacing (~622000 voxels for a volume of ~622 m^3) as they proved to be too computationally demanding for the 5 cm-spaced grid (which yields in terms of voxels alone a different order of magnitude, and additionally certain aspects of the analysis do not scale linearly).
3. To handle the different times since measurement of activity concentrations, all values were rescaled, so they represent the activity concentrations at the reference date, for which we used January 1, 2020.

Other outliers and/or errors were not present at first sight, and the representativeness of the data was judged to be sufficiently adequate for a first analysis., Although the boreholes were focused on one side of the biological shield, the liner data covered all walls, so at least some information (even if just secondary) on all parts of the biological shield was available, but it was not considered sufficient for meeting objective 1.C.

Table 2: Stage 1 data overview: Different types and corresponding amounts of data points, in the unfiltered dataset, gathered for constructing the 3D activity distribution maps during stage 1 of the project.

Data type		Parameter	Unit	Number of data points
Primary	Pre-existing (stage 1)	Ba-133, Eu-152, Co-60	Bq/g	184
Secondary	Pre-existing (stage 1)	Co-60	Bq/g	58 (pool liner data)

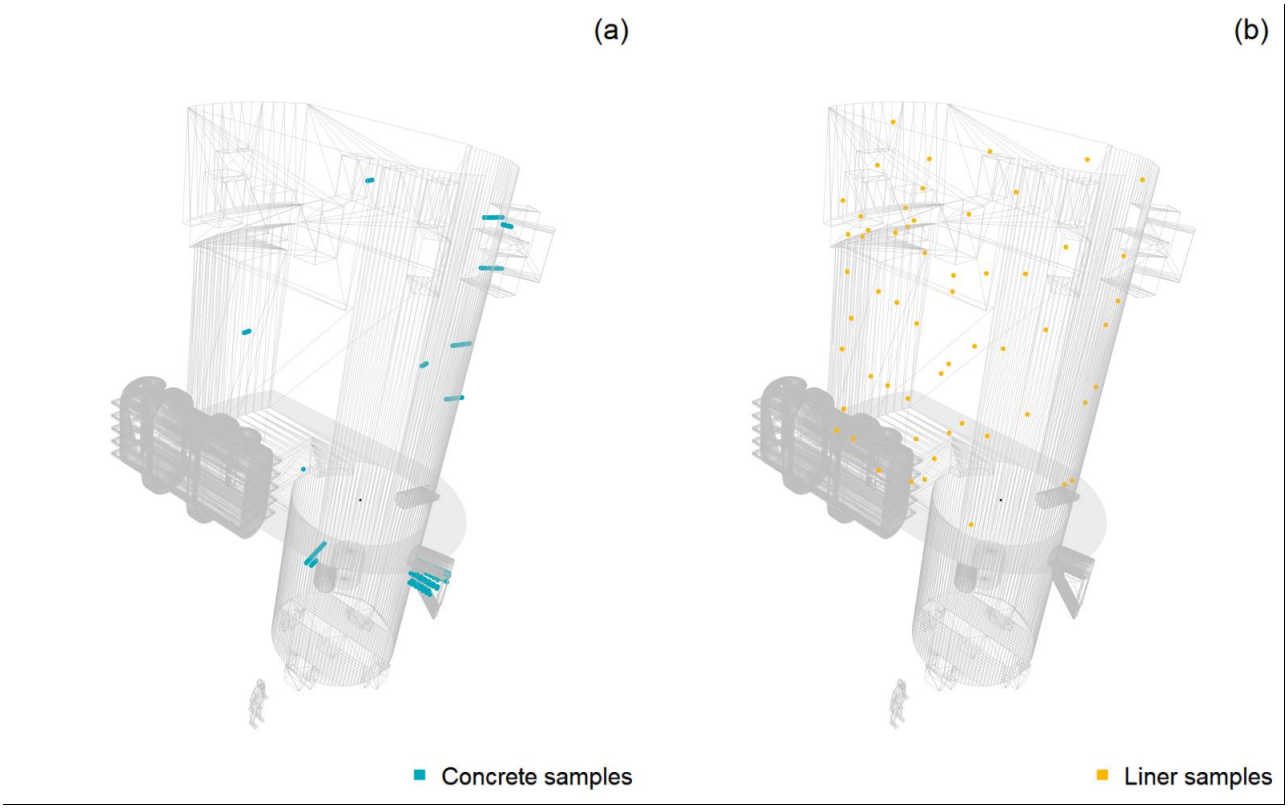

Figure 4: Overview of the borehole (a) and liner (b) data locations available during stage 1, and corresponding to the measurement results used in the preliminary data analysis.

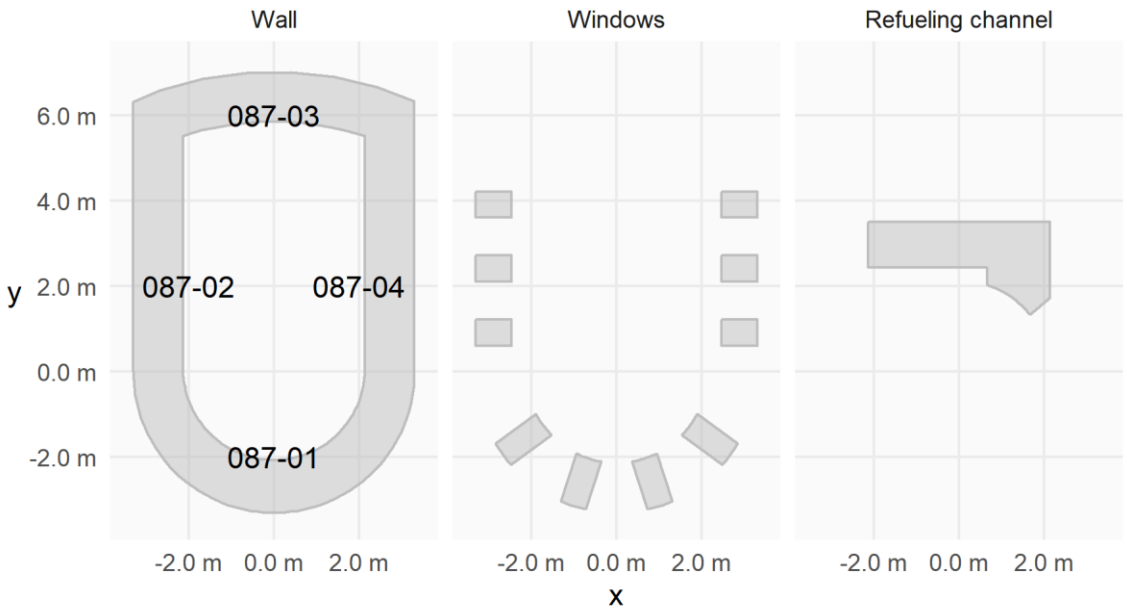

Figure 5: Horizontal cross sections through different parts of the biological shield. The wall cross section represents the wall thickness at the level of the reactor pool bottom (with an indication of the concrete element IDs; room number is 087, while the walls are numbered from 01 up to 04), while the windows are rectangular holes in the wall near the top of the structure, and the refuelling channel is an opening below the floor of the reactor pool.

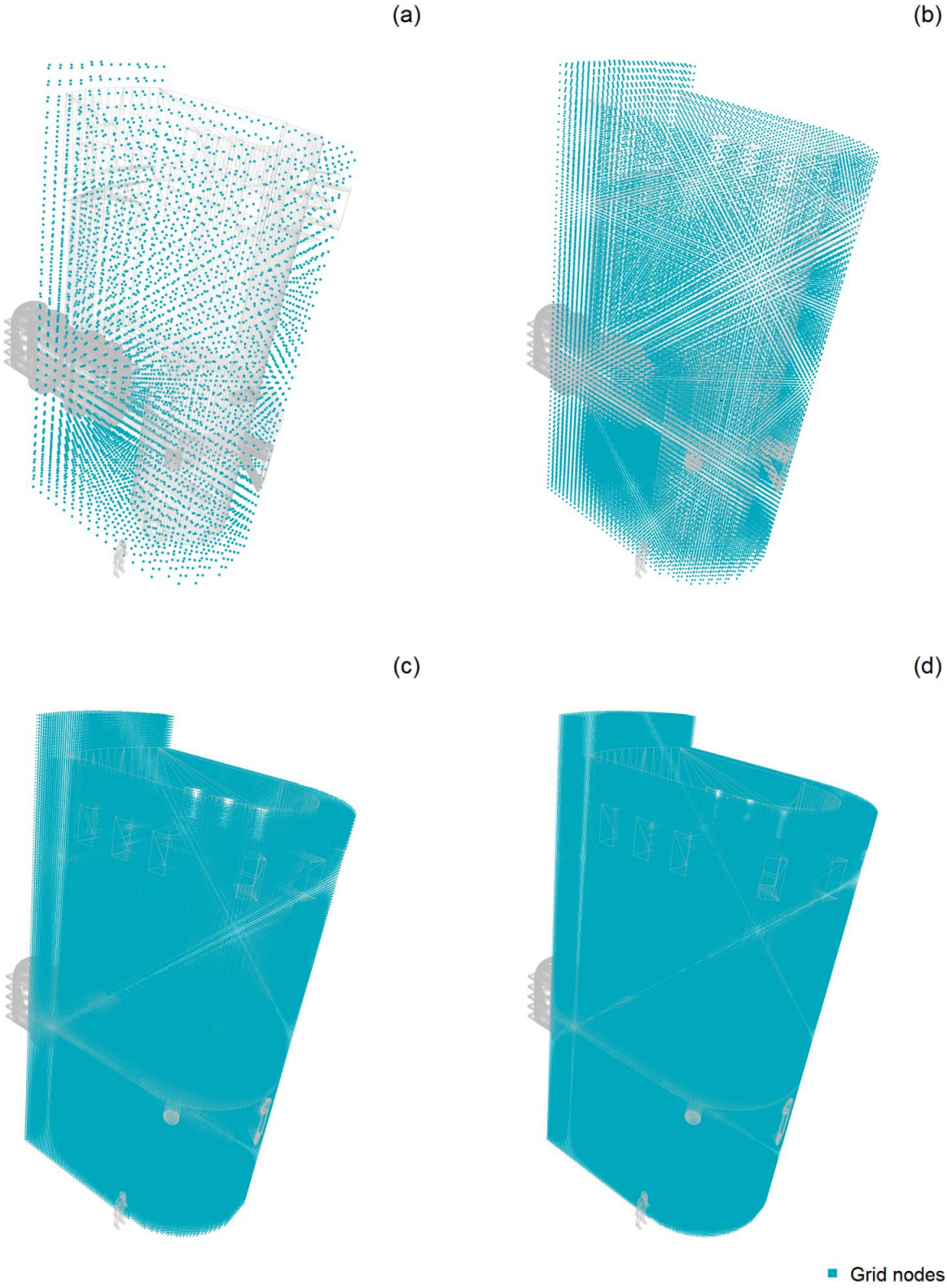

Figure 6: Different regular grids used for estimating the activity concentrations, with 50 (a), 25 (b), 10 (c) and 5 (d) cm spacing, corresponding to, respectively, ~4 700, ~41 400, ~622 000 and ~4 950 000 grid nodes.

2.2 Exploratory data analysis

During the exploratory data analysis, we focused on the **multivariate aspect**, and the potential relation between the liner activity concentrations and those in the concrete. It was already very clear from the start that there would be a **complex trend** related to the distance from the neutron source, and the depth in the concrete, and that characterization of this trend would be the main aim in this phase. If any **spatial structure** would be present, on top of the trend, it would **not** be **obvious** from the limited data in this case, and hence this was not further investigated. Furthermore, **robust approaches** were considered **out of scope** as well.

For the borehole analysis, an idea on the missing data and the pairwise correlations is provided in Figure 7. This clearly illustrates that we have Ba-133 results at all locations, but the other remaining radionuclides are not always available. The scatterplots and **correlations** on the other hand suggest that, certainly in this stage, we can focus on estimating Ba-133 activity concentrations, and derive the other values from this (*i.e.* using simple linear regression for the log-transformed values). Hence, we decided to **fall back to a univariate problem**, at least as far as the borehole data is concerned.

Since the **liner data** is **more systematically distributed** over the inner surface of the biological shield, we tried to account for it in this stage. In a later stage, when a similar distribution of borehole measurements would be available, accounting for this secondary data will not be so useful anymore. Indeed, from theory, we expect that the distribution of *e.g.* Co-60 activity in the liner provides some information on at least the relative distribution of Ba-133 activity concentrations at the concrete surface. Given the different spatial distribution of the liner and borehole data, it is however difficult to confirm this by an exploratory data analysis. We therefore do not discuss this relation here, but explain it as part of the workflow for the actual data analysis.

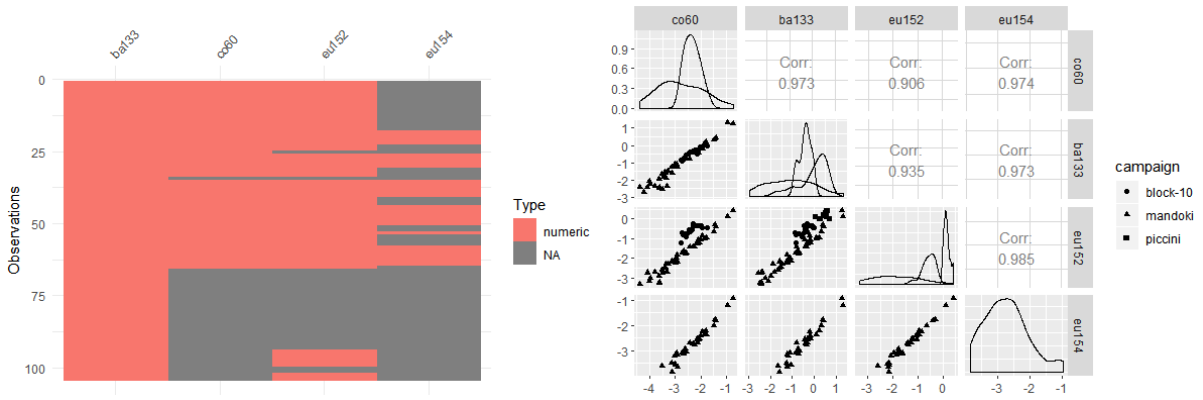

Figure 7: Preliminary stage 1 results: Overview of the borehole data. Left: indication on missing values. Right: scatterplot matrix of the logarithmic (base 10) activity concentrations.

2.3 Data analysis

We are thus focussing on modelling the complex trend of Ba-133 activity concentrations, and therefore we fall back, in accordance to the sampling design and data analysis strategy, to the **class of generalized linear models and potentially generalized additive models** if the former would not provide sufficient flexibility. Different features are available for use as regressors in this case. We considered the spatial coordinates, including the absolute x coordinate because of the expected symmetry (see Figure 9). In addition, the distance to the reactor fuel, the depth within the concrete, the spatial coordinates of the point projected to the inner surface of the biological shield, and the corresponding liner Co-60 activity concentration were considered as potentially informative.

The **liner Co-60 activity concentration** is **only available at the measurement locations**. Therefore, we used a **generalized additive model** to interpolate these measurements on the inner

surface of the biological shield, as a smooth function of the projected x and z coordinates, and the corresponding distance to the fuel. A linear model did not suffice, because of the non-linear relation of the Co-60 activity concentration with some of the considered regressors. The underlying idea here is that for every grid node in 3D, we can estimate the Ba133 activity concentration for the corresponding point at the inner surface of the wall, based on the Co-60 activity in the liner at that location. Figure 8 illustrates the results.

For similar reasons, the **trend modelling for the Ba-133 activity** concentrations was done with a **generalized additive model** as well, using a smooth function of the above estimated liner Co-60 activity concentration for all grid nodes and the depth within the concrete. The results of this model are illustrated in Figure 9. A comparison with the measurement data is provided in Figure 10. Although there are clearly still issues to be addressed, this already seems to provide an idea on the order of magnitude to expect across the entire volume of the biological shield and the features that seem related to the activity distribution (*i.e.* a measure of activation at the inner surface combined with the depth in the concrete wall), which is very useful for informing the sampling design.

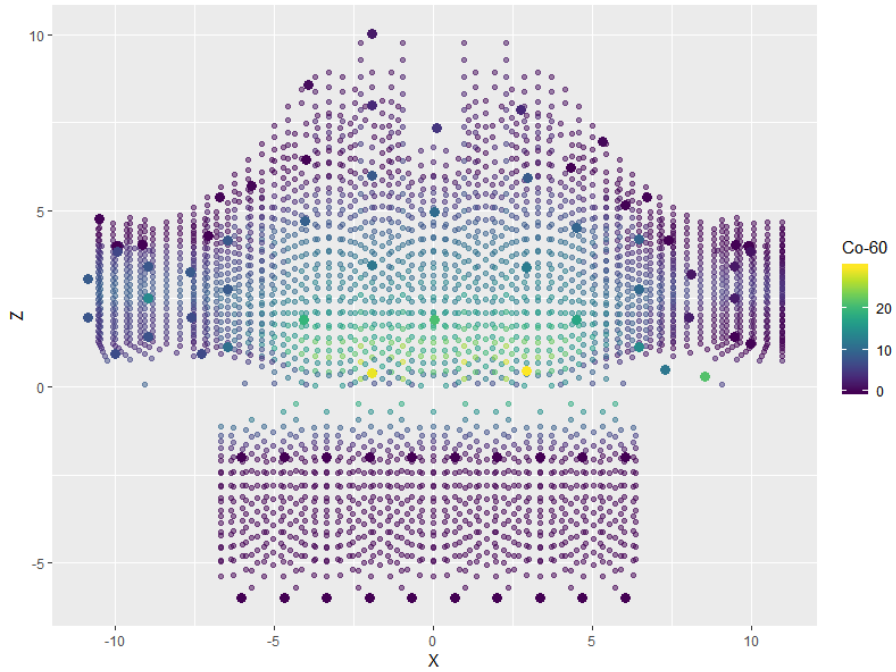

Figure 8: Preliminary stage 1 results: Overview of the liner Co-60 activity concentrations (large, non-transparent points) and the predictions of the generalized additive model (small, transparent points) for different points within the biological shield, based on an unwrapped projection to the inner surface of the biological shield.

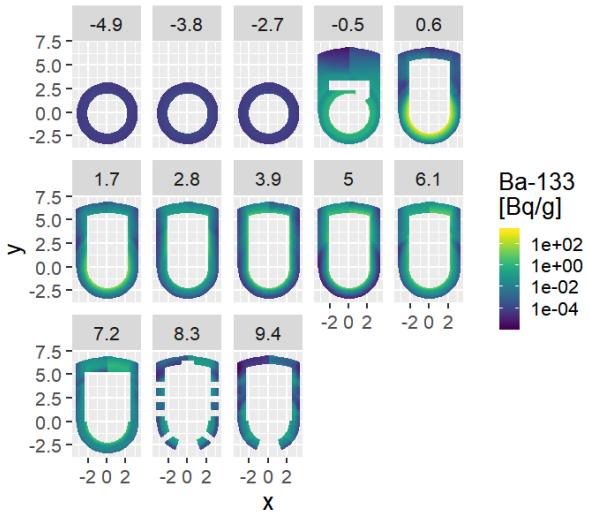

Figure 9: Preliminary stage 1 results: Series of horizontal slices through the preliminary Ba-133 3D activity concentration distribution maps, for different z coordinates.

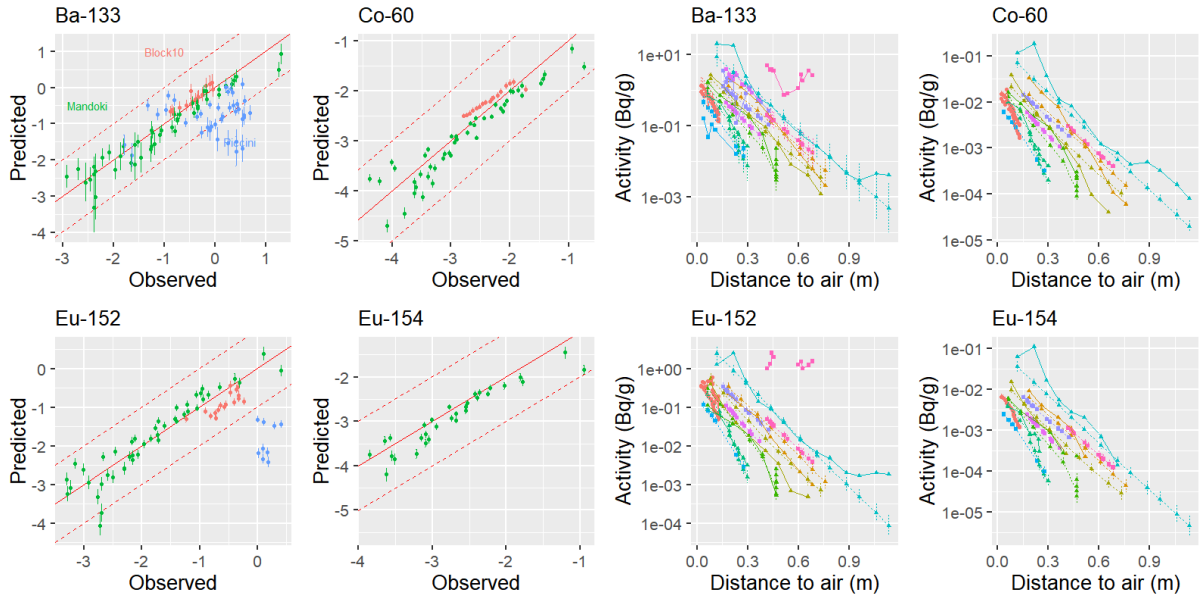

Figure 10: Preliminary stage 1 results: Overview of the predicted/fitted versus the observed data (for the logarithmic (base 10) transforms) (left four plots) and the results for the different boreholes, with observed values in solid lines and predictions in dashed lines (right four plots).

No post-processing was performed in stage 1 and a proper quantification of the uncertainties on the results was not considered relevant at this stage.

2.4 Sampling design

The sampling strategy consisted of the gathering of two types of data:

- Secondary data: quick, straightforward and cheap non-destructive in-situ measurements.
- Primary data: borehole sampling, sample preparation and in-lab measurements.

After removing the pool liner, we planned to perform an in-situ total gamma surface mapping, consisting of about one measurement per square meter or roughly nearly 300 individual

measurements (**secondary data**). We chose for regular grid sampling (Figure 11) to achieve full coverage, as the idea was to use these data as secondary information for the activity concentrations within the concrete, potentially in a similar way as how the liner data was used for the preliminary data analysis. As the in-situ total gamma surface mapping was directly perfomed on the concrete and consisted of a lot more data points compared to the liner data, the liner data was no longer considered in the stage 2 and stage 3 analyses.

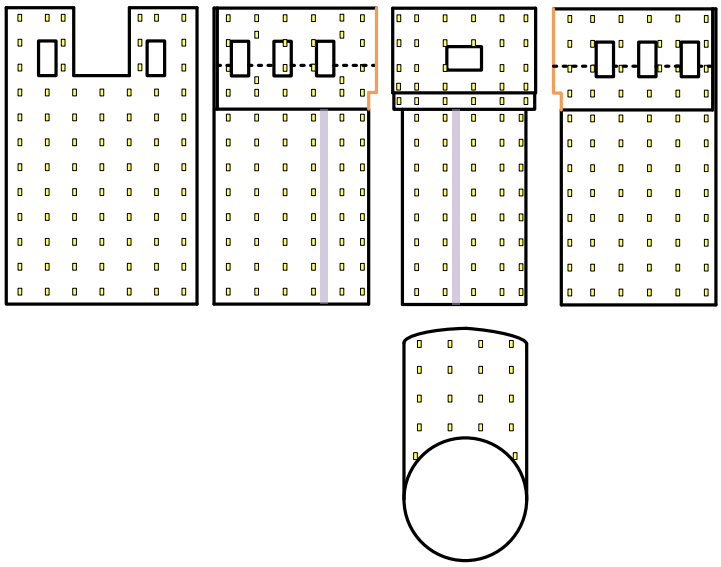

Figure 11: In-situ total gamma surface mapping of the inner pool (top) walls and floor (bottom). The yellow rectangles indicated the measurement locations

Following the basic principles as described in the INSIDER data analysis & sampling design strategy (Rogiers, et al., 2018) (Desnoyers & Rogiers, 2020), the sampling design for **the primary data** consisted of **systematic sampling** (equal probability of selection/probabilistic) **supplemented with judgemental sampling locations** (specific structures such as the reactor pool storage of reactor internals or “poubelle” and the refuelling channel and close to the location with the maximal activation level). In addition, the expected **trend extreme locations** were selected as well, and we relied on the symmetry of the activation to maximize the results with a minimum number of samples. Figure 12 shows the sampling plan.

This combination of sampling approaches basically ensured that:

1. We covered all the concrete elements, to reduce the risk of missing anything anomalous (addressing objective 1.C).
2. We included (approximately) the minimum and maximum values across the entire biological shield inner surface (not in depth), but also within every element, to reduce the required amount of extrapolation during the data analysis (addressing objective 1.C).
3. We investigated specific features for which it is known that they deviate from the general trend (addressing objective 1.A).

The part below the reactor pool bottom (NST pit) was not accesible for sampling at this point in time, due to the presence of a massive metal fixation ring in the NST pit wall.

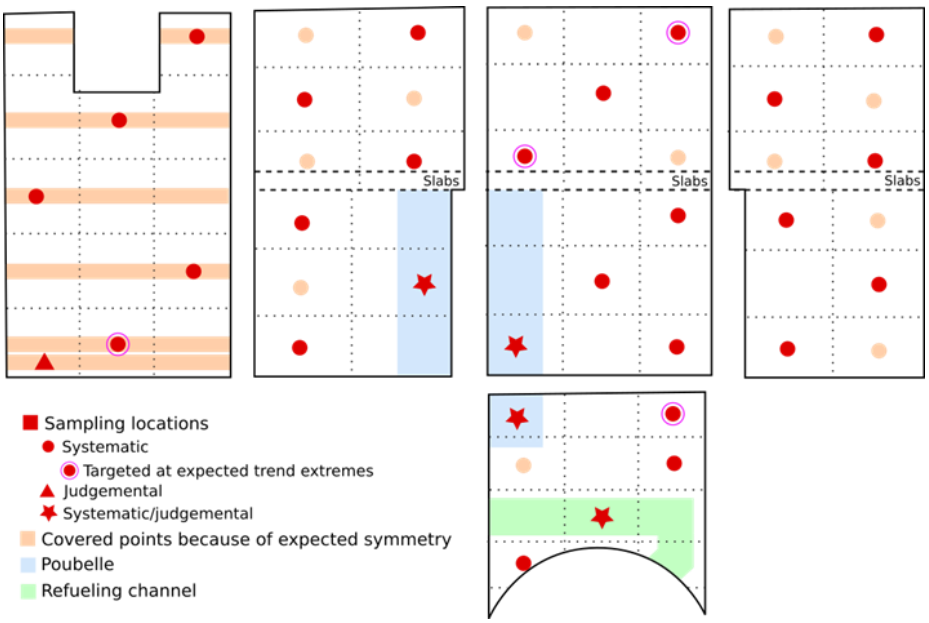

Figure 12: Sampling plan for the BR3 biological shield (30 samples).

3 Stage 2: Execution sampling plan, data analysis on the combined dataset & post-processing

The secondary data gathering was performed according to plan, using a Como 300G plastic scintillator a surface of 300 cm². For the primary data gathering, we took the 30 samples by wet core drilling **in agreement with the sampling plan**. The cores (diameter 72 mm, length of about 90 cm down at the backside reinforcement bars) were segmented (thickness of 5 to 10 mm) and some of those segments analysed by high-resolution gamma spectrometry in two consecutive steps. A total of 233 segments originating from the 30 drill core samples were analysed. In addition to the 30 samples, 6 cores (diameter 72 mm, length 30 cm) were taken and transported to the National Physical Laboratory for homogenisation and distribution to other EU laboratories. They serve as base material for the INSIDER benchmarking exercises (see section 5.2).

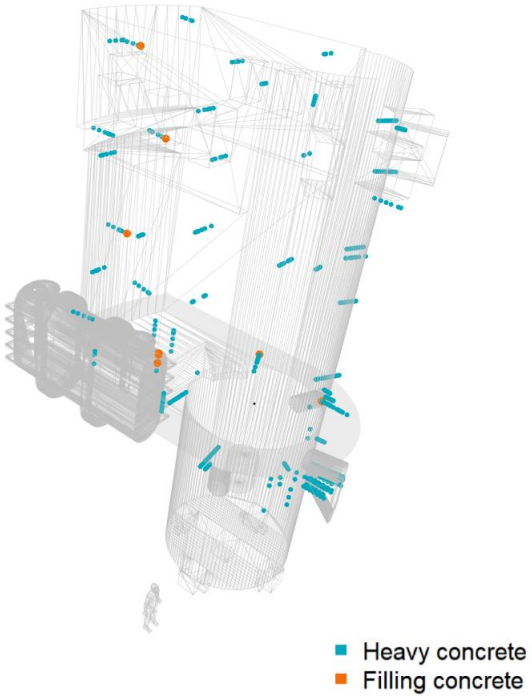

Figure 13

Table 3 and **Figure 14** give an overview of the primary and secondary data used for the stage 2 data analysis. The liner data used in the preliminary data analysis as secondary data were replaced by the 296 Como 300G data points, while the pre-existing primary data were extended with the results from the new samples and high-resolution gamma spectrometry.

Table 3: Stage 2 data overview: Different types and corresponding amounts of data points, in the unfiltered dataset, gathered for constructing the 3D activity distribution maps during stage 2 of the project.

Data type		Parameter	Unit	Number of data points
Primary	Pre-existing (stage 1)	Ba-133, Eu-152, Co-60	Bq/g	184
	New (stage 2)		Bq/g	206
Secondary	New (stage 2)	Total gamma	cps	296 (mapping)

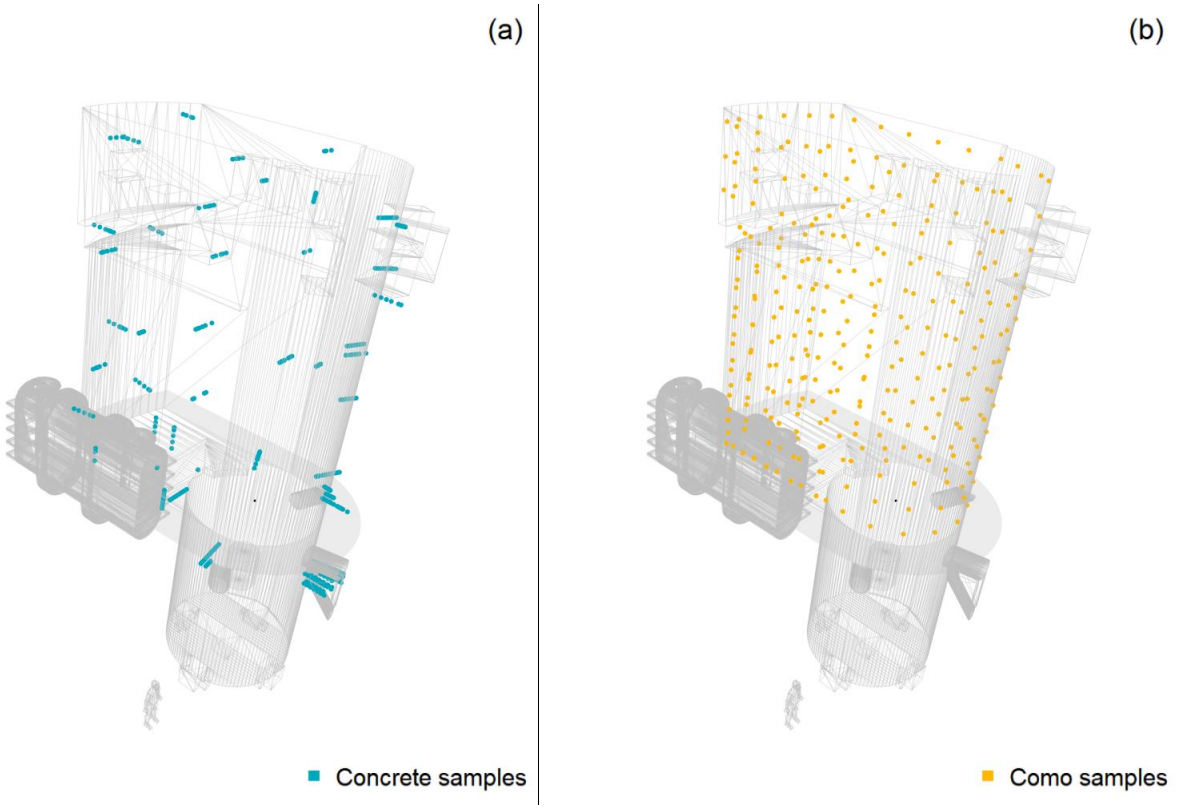

Figure 14: Overview of the borehole (a) and Como (b) data locations (2018 campaign) used in stage 2. The liner data used in stage 1 was superseded by the information provided by the Como dataset.

The **data analysis** on the stage 2 dataset resulted in 3D activity concentration distribution maps. We do not further present the results here since the **post-processing** showed a few unexpected and/or aberrant results and as a consequence the inability to reach the objectives (*i.e.* 1.B and 1.C). We identified **two areas**:

- Just below the bottom of the reactor pool, at the upper part of the **Neutron Shield Tank (NST) pit** (z (0, -2), see also Figure 9), the activity concentration levels were unexpectedly large, exceeding the limits for conditional release. We did not succeed to in-situ measure nor sample this region due to the presence of an activated metal ring that used to fix the NST. This led to a very uncertain extrapolation of the modelled results.
- The area around the "**poubelle**", as indicated in blue in Figure 12, showed unusual increased values. The measured results were probably influenced by an, at first sight, minor contamination in the proximity, potentially originating from the sampling of the liner.

The two areas were subject to further examination in stage 3.

Still worth mentioning here, however, is the adoption of training versus test sets for the different parts of the model during stage 2, whereas cross-validation was used for hyperparameter tuning when relevant, mainly because of the evaluation of non-linear versus linear regression approaches for the main Ba-133 activity concentration trend. Although the non-linear regressions proved to generalize better in terms of test set performance, there were lots of issues with extrapolation towards sections in the concrete volume far removed from the boreholes or inner surface of the bioshield (mainly deep in the NST pit and below the reactor pool floor), bringing problems for objective 1.B. Hence, it was decided to continue with linear trend models, which also were more convenient in terms of the evaluation of uncertainties by simulation, and accept somewhat reduced predictive power close to, or at, the actually measured locations. Following the correspondingly reduced risk for overfitting, we decided to abandon the train/test split (although in most, not all,

cases test set performance was a bit lower than for the training set, the numbers were actually very similar), and work on the full dataset in stage 3, where cross-validation was envisioned in any case (see Section 4.3).

4 Stage 3: Additional data gathering & data analysis on the final dataset

The D&D staff performed two preparatory actions prior to the additional data gathering in stage 3: 1) dismantling of the metal fixation ring on top of the NST pit and 2) decontamination of the pool floor hot spot in the neighbourhood of the poubelle. The additional data gathering was then performed, and was followed by a data analysis on the entire dataset. The deterministic estimate from stage 2 was then replaced by a probabilistic reference case. Furthermore, a limited sensitivity analysis was performed, based on a set of discrete cases with respect to the uncertainties accounted for, and the amount of available data.

4.1 Additional data gathering

Since the effort was rather limited, we decided to **repeat** the in-situ total gamma surface mapping now the metal ring and contamination were removed, increasing the measurement density at some of the **critical areas** (e.g. area z (0,-2) in the NST pit, especially around the legs of the primary circuit). This resulted in an entire new secondary dataset consisting of 399 individual Como 300G measurement results, which was considered higher quality because of the decreased potential for influencing background radiation. A few measurements close to the refuelling channel of the 2018 campaign that were not redone, but still provided information on interesting points were corrected for decay and possible background radiation effects using the robust linear model presented in Figure 15.

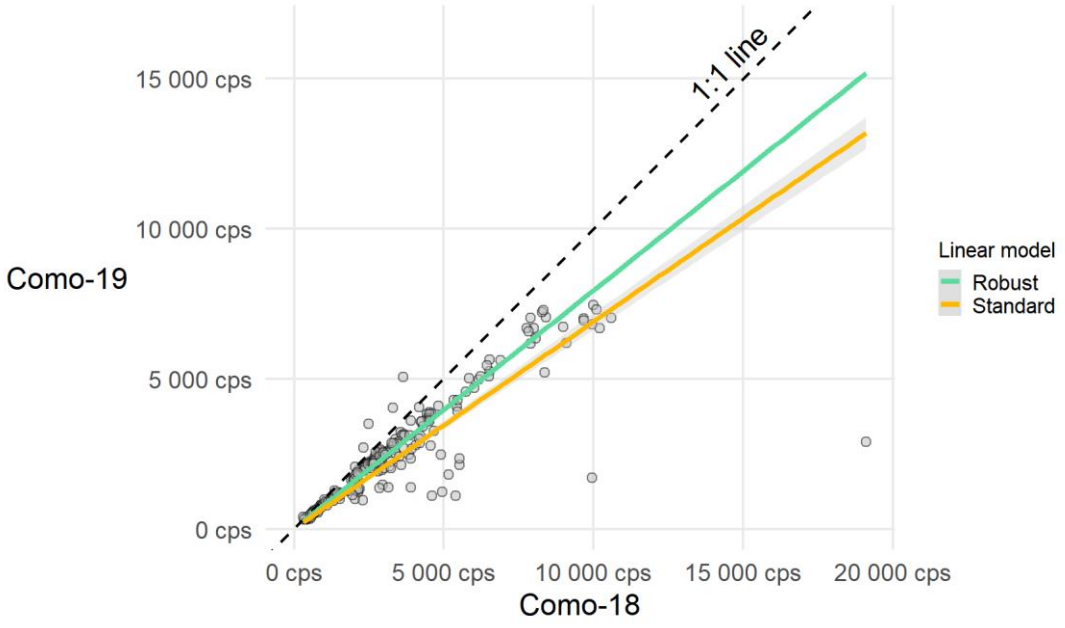

Figure 15: The few data points from the Como 2018 campaign (Como-18) that were not measured again during the 2019 campaign (Como-19) were corrected for decay and potential background radiation effects using a robust linear model (as several outliers were present given the metal ring and local contamination), which resulted in count rates consistent with the 2019 campaign, of about 79% of the original 2018 count rates.

Furthermore, we drilled 13 holes of 30 cm depth in the area between 0 and -2 m in the NST pit using an ordinary Widia drill. The dust from each drill hole was collected and control measurements were performed using high-resolution gamma spectrometry. For four drill holes, the activity concentration at six different depth locations was established based on the determination of

the activity profile inside each hole using a CZT detector for acquiring a count rate as a function of depth and combining the profile with the result of the Ba-133 activity concentration determination in the dust sample measurement. This resulted in 25 additional data points. Table 4 and Figure 16 give an overview of the final dataset, consisting of a total of 824 data points: 415 primary and 419 secondary data points.

Table 4: Stage 3 (final stage) data overview: Different types and corresponding amounts of data points, in the unfiltered dataset, gathered for constructing the 3D activity concentration distribution maps during stage 3 of the project.

Data type		Parameter	Unit	Number of data points
Primary	Pre-existing (stage 1)	Ba-133, (Eu-152, Co-60)	Bq/g	184
	New (stage 2)	Ba-133, Eu-152, Co-60	Bq/g	206
	Additional (stage 3)	Ba-133	Bq/g	25
Secondary	New (stage 2)	Total gamma	cps	20 (of 296)
	Repeated (stage 3)	Total gamma	cps	280
	Additional (stage 3)	Total gamma	cps	119

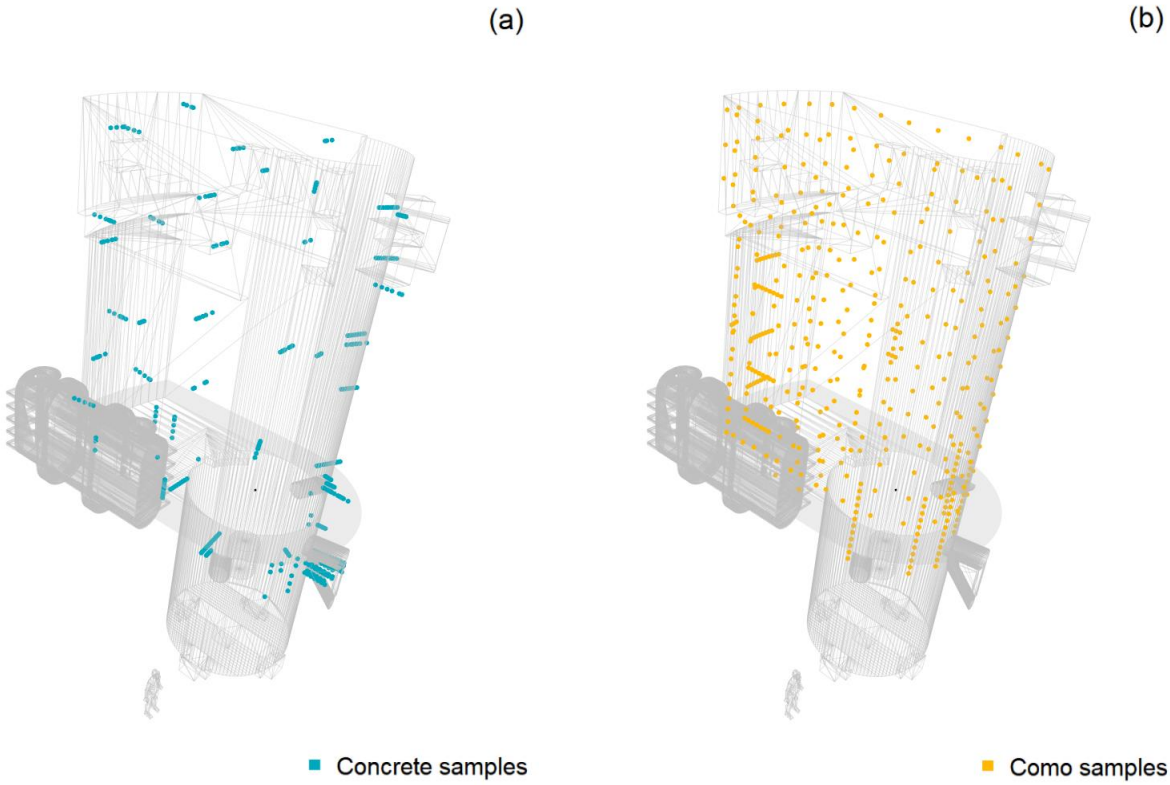

Figure 16: Overview of the borehole (a) and Como (b) data locations used in stage 3.

4.2 Data analysis on the entire dataset

As a start, the different measurement results were integrated into a deterministic 3D model. In a second step, the model was extended to a probabilistic one, that enabled the simulation of different kinds of uncertainties. The consideration of all realistic uncertainties was considered the reference case. For this reference case, the averaging was studied in detail, and reimplemented several times, targetting the best outcome under the constraints of the different regulations. Finally, spatial

categorisation was done on the optimal averaging results, leading to maps with *i.a.* spatially localised volumes destined for conditional or unconditional release. The different steps are discussed in detail below.

4.2.1 Integration of different measurement results in a deterministic 3D model

Figure 17, Figure 18 and Figure 19 illustrate the workflow of the primary and secondary data integration resulting in activity concentration estimates for each of the ~622k voxels of the biological shield, for Ba-133, Eu-152 and Co-60 respectively. For Ba-133, the approach works as follows (Figure 17):

- The 2018 and 2019 total gamma campaigns were combined using a robust linear model, as described in Section 4.1, resulting in 399 data points from the 2019 campaign, and 20 additional 2019 equivalents, from the 2018 campaign.
- Estimation of the Ba-133 activity concentration (Bq/g), using the total gamma measurement results (COMO 300G, cps):
    - Both datasets were joined using a nearest neighbour search (Figure 20), and subsetting the combinations by requiring a maximum distance of 0.5 m between the two data points, and a maximum depth in the wall of 5 cm for the borehole sample. Additionally, we restricted the combinations to Ba-133 activity concentration above $10^{-1.1}$ Bq/g to avoid some outliers that were clearly related to anomalous features, where the surface activities were apparently not in line with deeper activation levels (mainly behind the so-called “poubelle”),
    - A log-log linear model was used on the subsetted dataset to estimate Ba-133 activity concentrations for the full total gamma surface measurement dataset (Figure 21a),
- Determination of the Ba-133 activity concentration (Bq/g) for each of the voxels:
    - All different Ba-133 data sources were combined, including the Ba-133 estimates based on total gamma measurements,
    - All Ba-133 activity concentrations were log-transformed, as they vary over orders of magnitude, and we are clearly dealing with log-linear trends with the depth in the wall, as was already evident from the pre-existing data, and confirmed by the new measurements,
    - A linear trend model was fitted (Figure 21b), using the following, partly physically-based features as regressors:
        - For the attenuation of the neutron radiation within the concrete wall, we use simply the depth inside the concrete as a regressor (which results in the observed log-linear trends mentioned above),
        - For accounting in a simplified way for the presence on the neutron shield tank inside the NST pit, we use the depth below the pool floor level as an additional regressor (resulting in another log-linear trend),
        - For accounting for the location of the source of the neutrons, we use the logarithm of the squared inverse distance to the fuel as additional regressor, which corresponds to an approximation of the decrease in neutron flux using the inverse square law,
        - And finally, since it is known there are some activation anomalies around the hot and cold legs, as they created an opening in the NST, we consider these as additional “sources” of neutrons, and use the logarithm of the squared inverse distance to any of the legs to allow for locally increased activation levels,

- Using the same features for all the voxels of the biological shield, the Ba-133 trend was estimated everywhere using this model,
- The residuals of the Ba-133 trend model showed clear heteroscedasticity, and hence the variance was rescaled according to the Ba-133 trend level (Figure 22a), and Gaussian anamorphosis was applied using ordered quantile normalization.
- These transformed residuals showed clear spatial correlation (Figure 22b), and hence they were further treated with simple kriging, to come up with estimates of the residuals for all voxels of the biological shield, after which the reverse transformation was performed,
- The trend and residual estimates were added for all voxels, resulting in the final Ba-133 activity concentration estimates.

For Eu-152, the approach is more straightforward, as we make use of the Ba-133 estimates (Figure 18):

- All different Eu-152 data sources were combined,
- All Eu-152 activity concentrations were log-transformed for the same reasons as Ba-133,
- The samples with both Eu-152 and Ba-133 values were split into two groups, depending on the concrete type,
- For each group, a scaling model was fitted (log-log), to estimate Eu-152 from Ba-133 (*i.e.* a scaling factor approach using Ba-133 as key nuclide),
- Using the Ba-133 estimates and concrete type for all the voxels of the biological shield, the Eu-152 trend was estimated everywhere using these two models,
- After checking that the Eu-152 residuals were not correlated with the Co-60 residuals (Figure 24a), Gaussian anamorphosis was applied to the Eu-152 residuals using ordered quantile normalization,
- The transformed residuals showed clear spatial correlation (Figure 24b), and hence they were further treated with simple kriging, to come up with estimates of the residuals for all voxels of the biological shield, after which the reverse transformation for undoing the Gaussian anamorphosis was performed,
- The trend and residual estimates were added for all voxels, resulting in the final Eu-152 activity concentration estimates.

For Co-60, the approach is basically the same as for Eu-152, except for the fact that there is no clear distinction between the red and grey concrete types, which justifies use of a single trend model to estimate Co-60 based on Ba-133, instead of two (Figure 19).

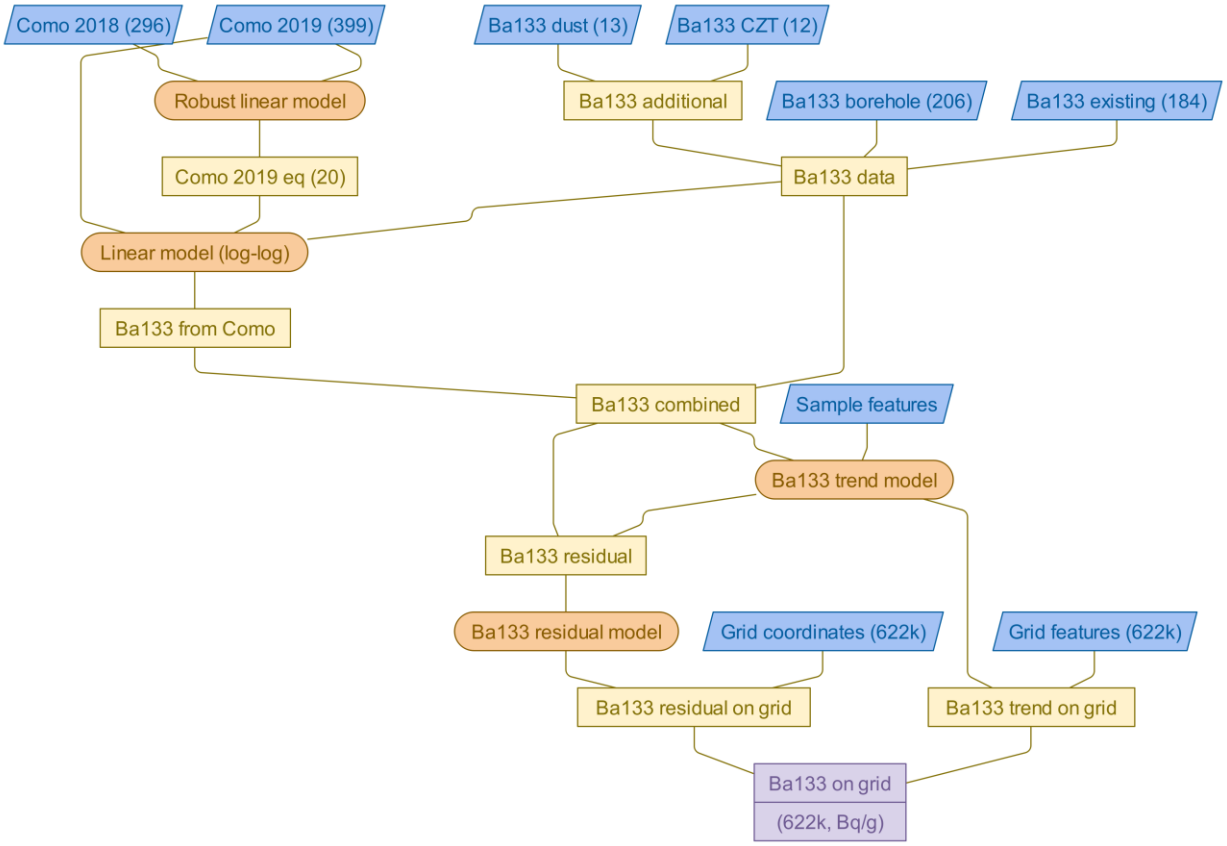

Figure 17: Overview of the workflow to transform the measurement results into estimates of Ba-133 activity concentration over the grid representing the bioshield concrete.

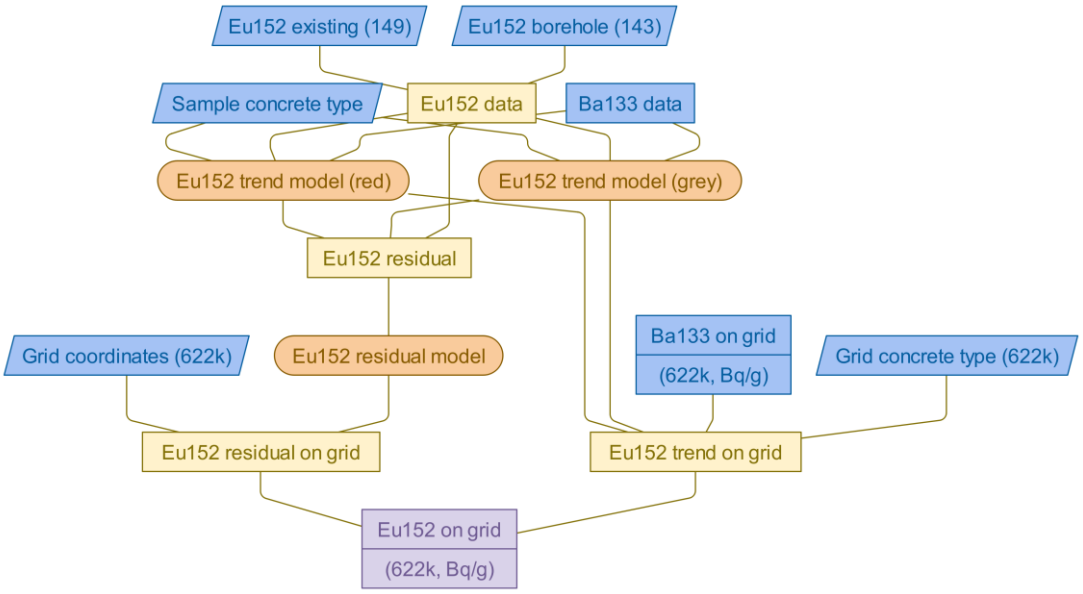

Figure 18: Overview of the workflow to transform the measurement results into estimates of Eu-152 activity concentration over the grid representing the bioshield concrete.

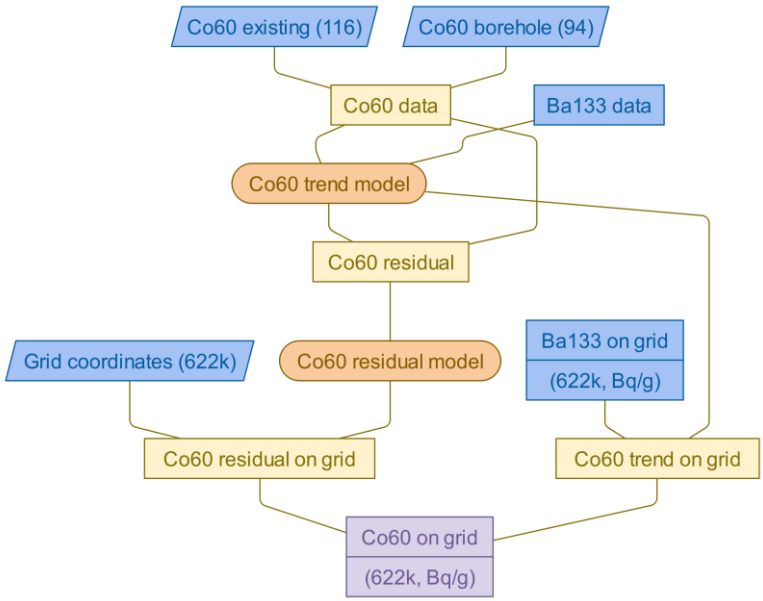

Figure 19: Overview of the workflow to transform the measurement results into estimates of Co-60 activity concentration over the grid representing the bioshield concrete.

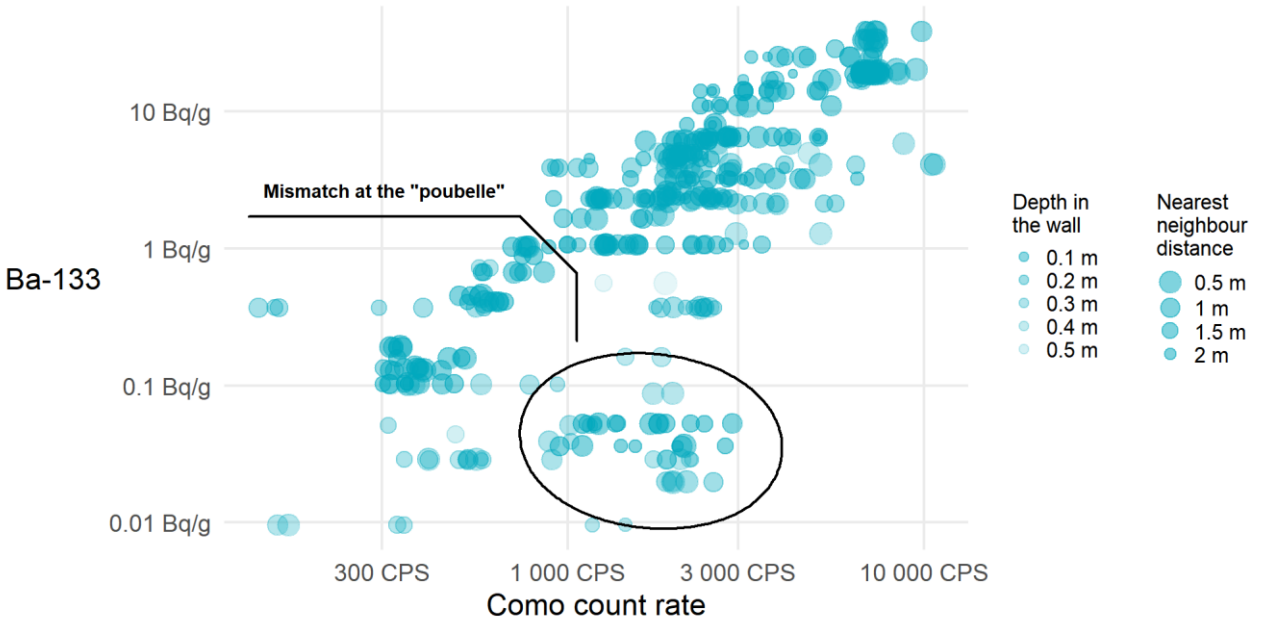

Figure 20: Ba-133 activity concentrations from the borehole samples versus total gamma count rates corresponding to their nearest neighbours.

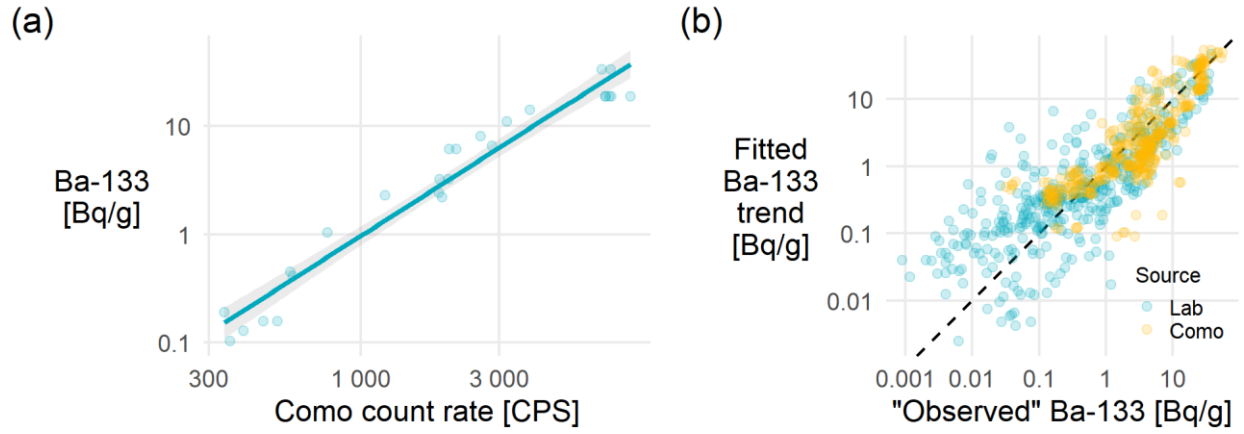

Figure 21: Subsetted dataset of nearest neighbour matches between borehole samples and total gamma surface measurements, and the fitted linear model (log-log) (a), and fitted Ba-133 trend versus the measured activity concentrations, and those estimated based on the total gamma surface measurements (b).

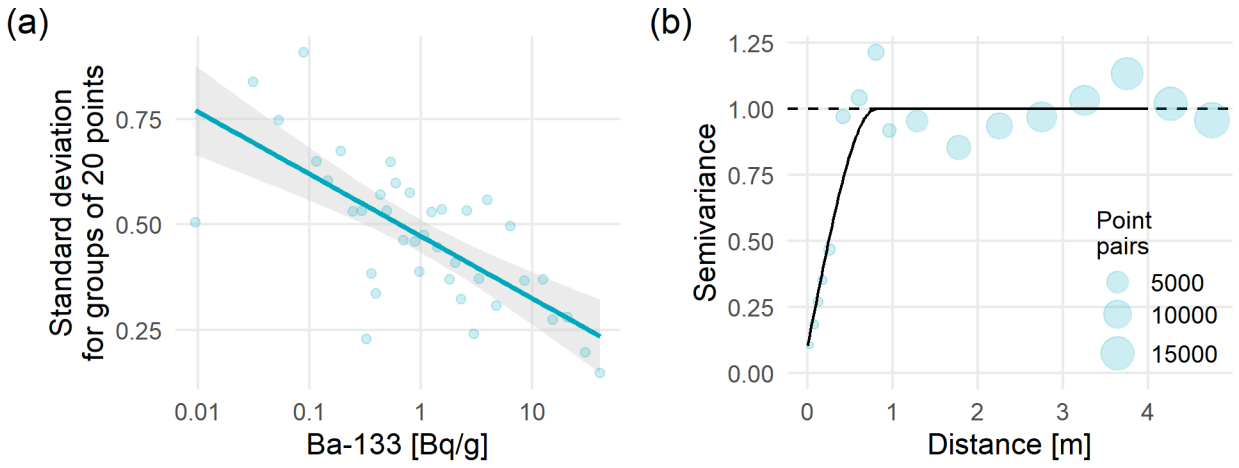

Figure 22: Illustration of the heteroscedasticity, and the standard deviation estimate used for rescaling (a), and the experimental and modelled variograms for the rescaled Ba-133 residuals (b).

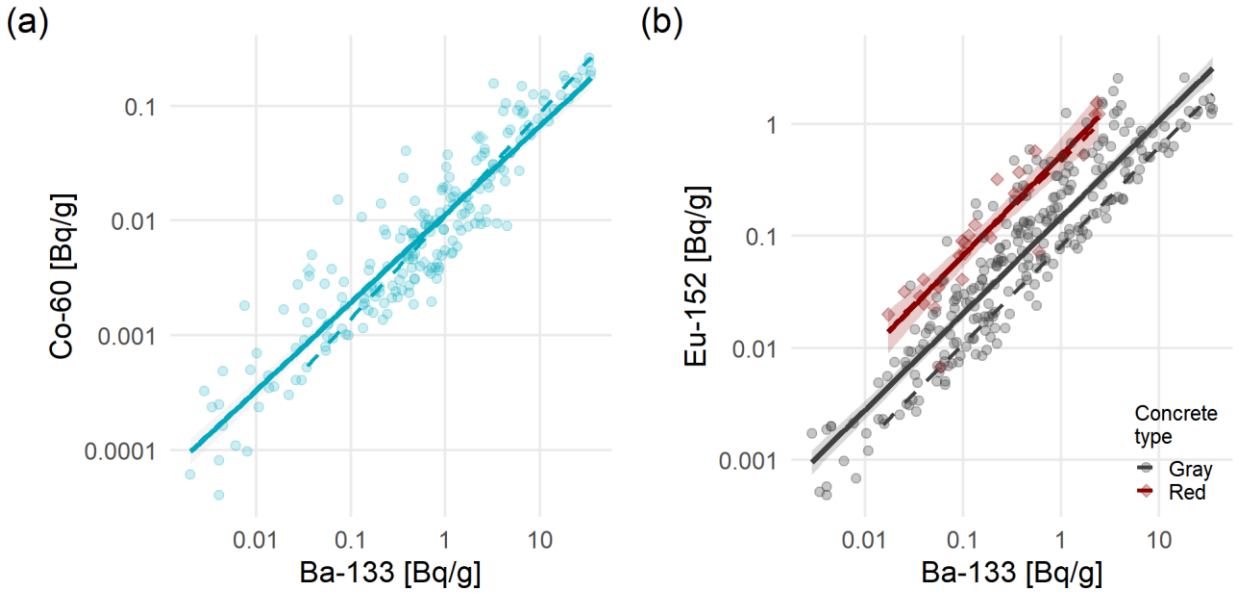

Figure 23: Scatterplots for Co-60 (a) and Eu-152 (b) versus Ba-133 activity concentrations, and the corresponding linear model fits (log-log). For Eu-152, there are two linear models, corresponding to the two main types of concrete used for the biological shield. The dashed lines provide an idea on how the fit would change in case only the subset of 15 boreholes is considered (see Section 4.3.2).

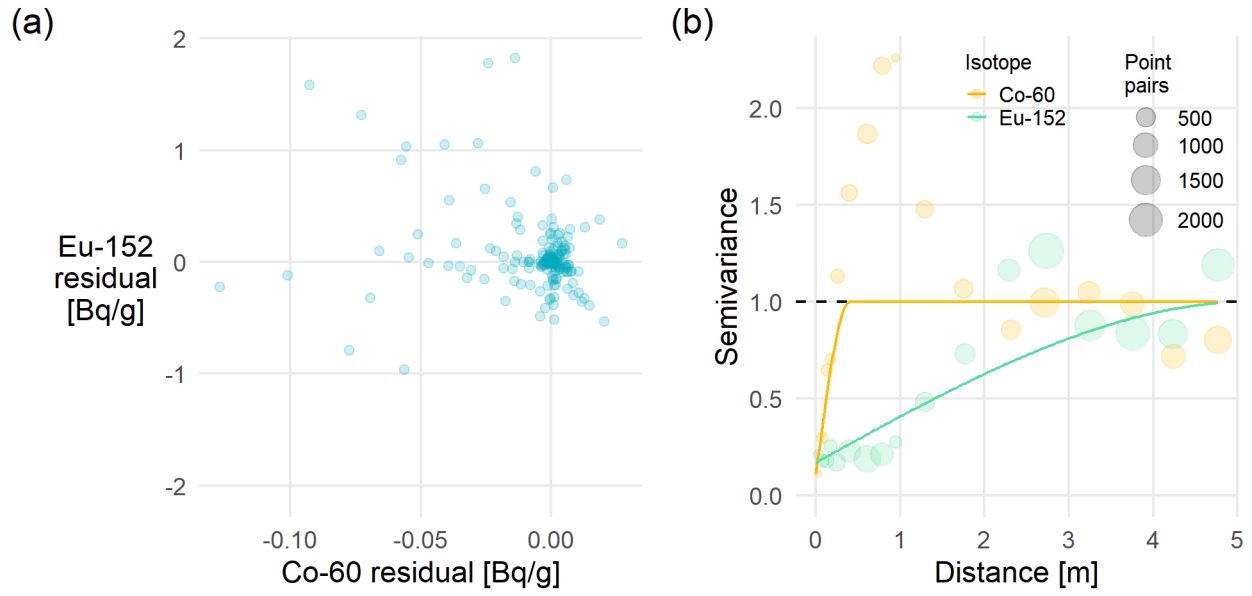

Figure 24: Scatterplot of the Eu-152 versus the Co-60 residuals (a), and experimental and modelled variograms for the rescaled Co-60 and Eu-152 residuals (b).

4.2.2 A probabilistic model to account for uncertainties

As the simple kriging of the residuals of the Ba-133, Eu-152 and Co-60 trend models provides only best linear unbiased estimates on a voxel level, an extension of the above approach is required if we do want to look into averaging over blocks of 0.66³ m³. Moreover, in line with objective 1, we need to account for at least the major uncertainties to be able to judge whether we consider the results sufficiently reliable or not. To that end, the above deterministic approach was extended to a probabilistic model in the following ways:

- Measurement error (percentages mentioned represent relative expanded uncertainty with coverage factor 2, *i.e.* two standard deviations)
    - The total gamma measurement results were perturbed with a random error of 5% (as systematic errors here are of no influence because we use these as secondary data). This random error is based on the results for the Como300G in the UC2 on-site intercomparison exercise (section 5.1),
    - The activity concentrations were perturbed with a systematic error of 10% and a random error of 10%, for each isotope separately. At the time of performing this calculations, the results of the UC2 intercomparision exercise (section **Error! Reference source not found.**) were not yet available. Moreover, the geometry of the sample measurements was not the same. We therefore roughly doubled the expanded uncertainty reported by the ISO 17025 accredited laboratory that performed the sample measurements,
- Linear models for 1) total gamma count rate to Ba-133 activity concentration translation, 2) Ba-133 trend estimation, 3) Eu-152 trend estimation (scaling factor approach) and 4) Co-60 trend estimation (scaling factor approach)
    - Simulation of the systematic uncertainties was done based on the covariance matrix of the coefficient estimates,

    - For the total gamma count rate to Ba-133 translation, we added a random perturbation based on the residual variance of the model fit,
    - For the Ba-133 trend, we included the option to use heteroscedasticity-consistent covariance matrix estimation
- For the spatially correlated Ba-133, Eu-152 and Co-60 trend residuals,
    - Instead of simple kriging, we use the corresponding sequential simulation approach to obtain realizations of the random field that honour the spatial correlation models

We consider the probabilistic model with the above uncertainties as our reference case. For additionally enabling the evaluation of the effect of the residual spatial correlation models, we also implemented the options to:

- Perturb the fitted range of the variogram with an error of 50%, and
- Increase the relative nugget effect of the variogram by a random number between 0 and 10%,

which are only used during the senstivity analysis discussed in Section 4.3.

4.2.3 Optimal averaging under the imposed constraints

Objective 2 states that the volumes corresponding to the final categorisation should be optimised in an economical sense (meaning preferably less conditional, and more unconditional release). While there is no room for any optimisation within the probabilistic activity concentration modelling, we do have the option to look at averages over 0.66^3 m³ blocks to demonstrate compliance with the regulatory thresholds according to the sum formula.

However, since we are, at least locally at the scale of 0.66^3 m³ blocks, dealing with mainly a log-linear trend with the depth inside the concrete wall, considering arithmetic averages over blocks centered around a certain voxel, will in most cases lead to an increase of the average sum with respect to the sum for the center voxel (Figure 25).

Hence, to make use of the averaging option, we need a more complex operation. For every single grid node, we basically have to consider all 0.66^3 m³ blocks in which it is contained, and take the minimum of the resulting block average sums. The averaging step required a vector of grid node indices of maximum length 343 for 979k nodes, of which a considerable part is located outside of the concrete. For taking the minimum, similar grid node index vectors where then required for the 622k grid nodes within the concrete. The result of this operation is displayed in Figure 26.

Now most of the block average sums are below the grid node sums, but still for a part, the averaging results in larger values. Hence, we considered a final step, to take the minimum of the grid node sum and the corresponding minimum block average sums, making sure the averaging operation is only used in case of a positive effect (Figure 27).

Figure 28 provides on overview of the corresponding workflow, and the resulting classification into one of the two end stage volumes.

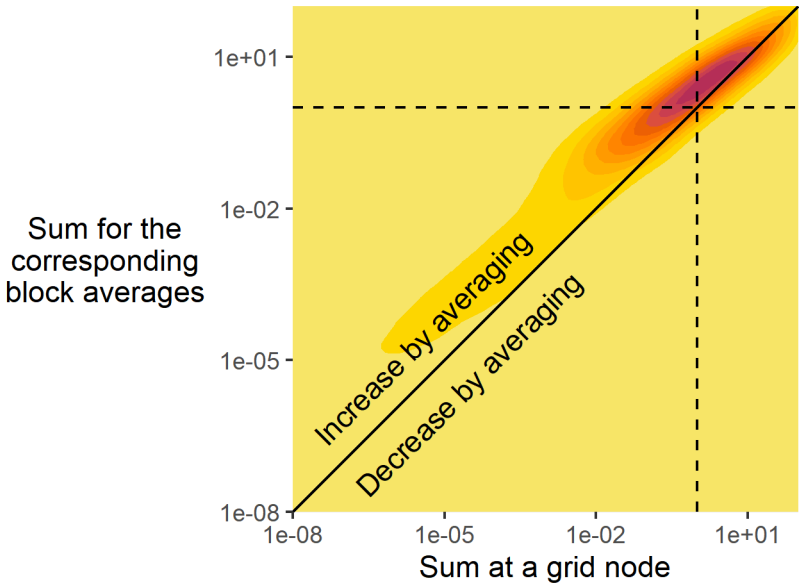

Figure 25: Two-dimensional density estimate for the block average sums versus the grid node sums at the center of the respective blocks.

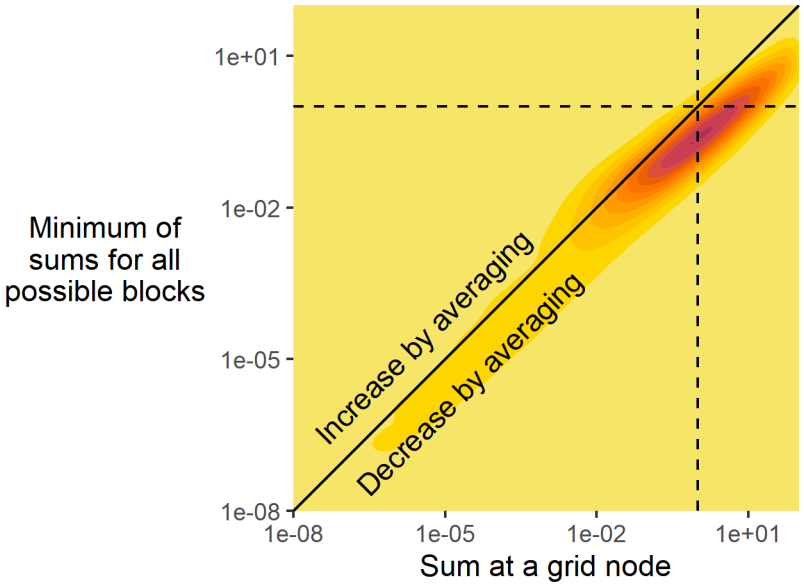

Figure 26: Two-dimensional density estimate for the minimum of sums for all possible blocks versus the grid node sums.

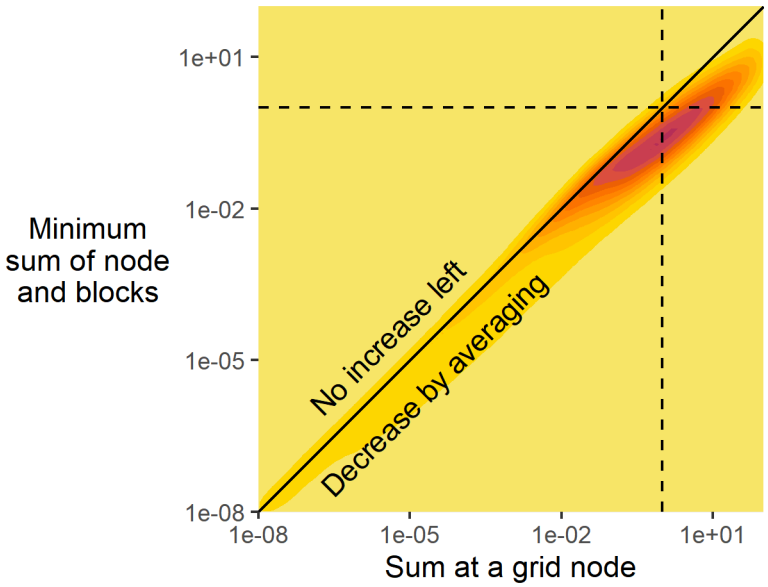

Figure 27: Two-dimensional density estimate for the minimum of sums for all possible blocks and the considered grid node, versus the grid node sums. Note that the density estimate seems to suggest some points are above the first diagonal, but this is an artifact of the visualization. All points above the diagonal in Figure 26 are placed exactly on the diagonal in this case.

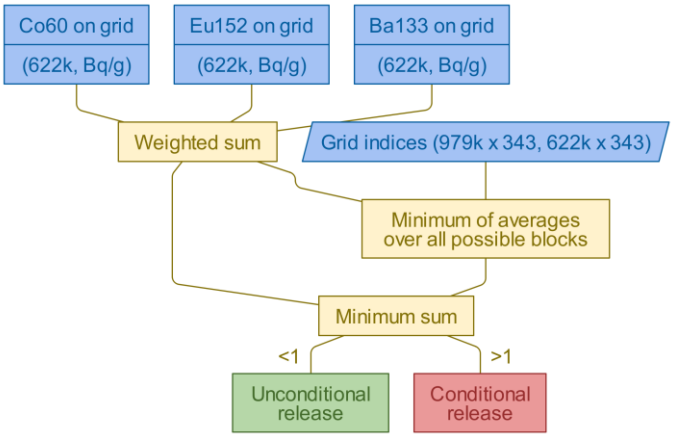

Figure 28: Overview of the workflow to transform the activity concentration estimates over the entire grid into corresponding minimum sum formula values, and finally a categorisation into one of the two end stage volumes.

4.2.4 Spatial categorisation of the final result

Following objective 3, quantification of the different end stage volumes is required, as well as spatial localisation. The former will be discussed in Section 4.3, while for the latter a dedicated series of detailed PDF exports of all horizontal slices through the biological shield grid was made available (not shown here) for further discussion on material separation options etc. To provide an overall idea of those results, Figure 29 provides a smaller set of horizontal slices, for every 0.5 m, for both the best estimate and conservative estimate, which are defined as the median and 95th percentile of a set of 100 simulations for the reference case.

Using the median as our “best” estimate basically means that in half of the biological shield, we would underestimate the volume to be removed, while in the other half, we would overestimate it. Generally speaking, however, this should give us the most accurate idea on the actual volume in which the threshold is exceeded, on a grid node basis, and the corresponding total activities.

By using the 95th percentile as our "conservative" estimate, we fare basically overestimating the volume to be removed in 95% of the biological shield, while only in 5%, we would underestimate it. Hence, this case is not relevant for estimating the actual radiological inventory, but it is useful to build in some conservatism with respect to the categorization, and corresponding planning for material separation etc.

Based on Figure 29, it seems that it won’t be necessary to remove material on top of the reactor pool (Figure 29b, top wall, last two slices). The zone labelled as conditional release is slowly thickening towards the bottom of the reactor pool. Above and just below the pool of the reactor pool, the full thickness of the pool wall needs to be removed, if we want to build in some conservativism (Figure 29b, second row, middle slices), while chances are actually not very likely that the activity concentrations at the outer surface of the wall will result in exceedance of the threshold, except maybe at the hot and cold legs and the windows high up in the wall which all enabled neutrons to move through easily (Figure 29a, second row fourth slice, and bottom row, first three slices).

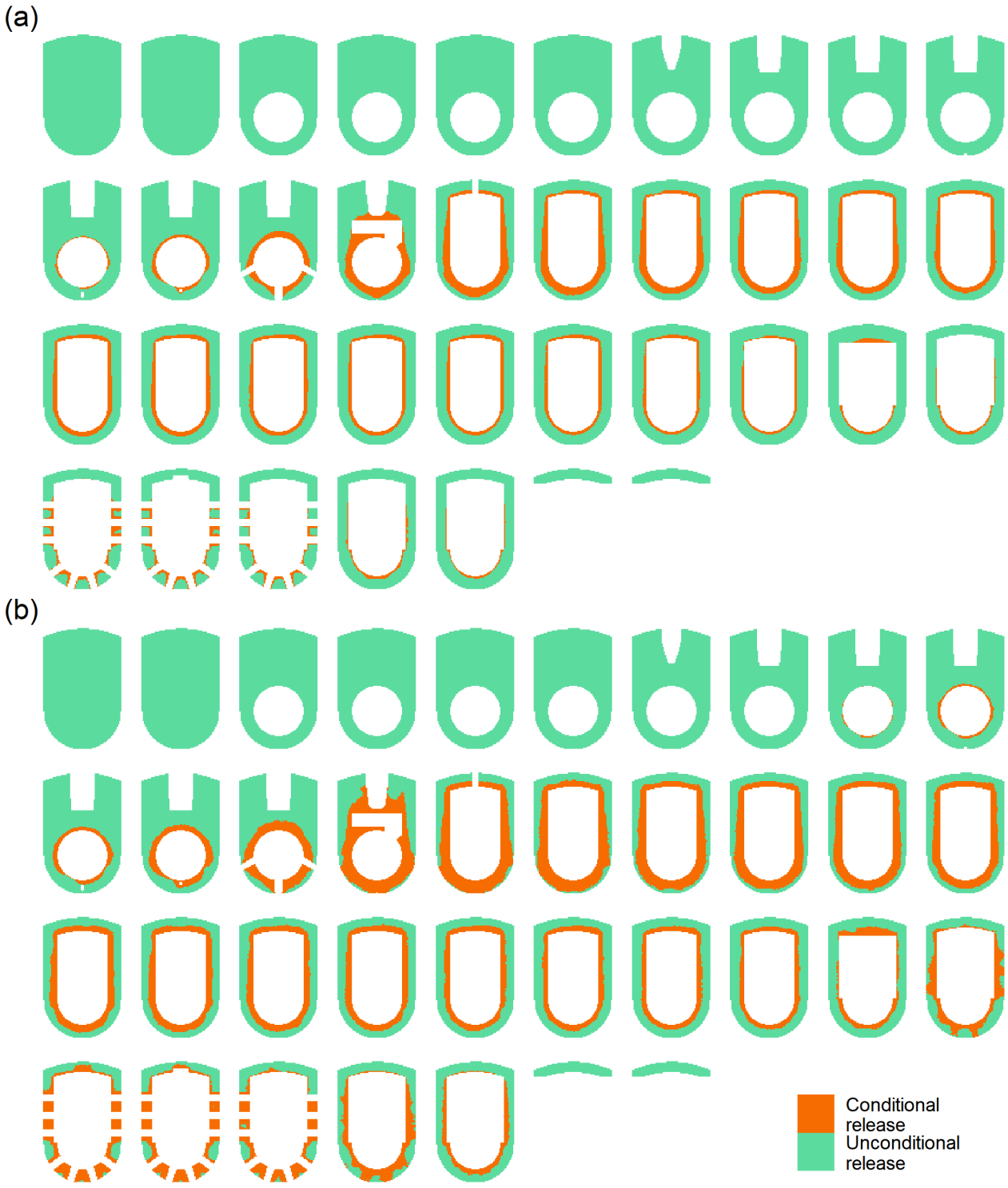

Figure 29: Horizontal sections of the biological shield for different z-values (every 50 cm). On top (a) we show the best estimate categorisation (median of the reference case), while the bottom figure (b) shows the conservative estimate categorisation (95th percentile of the reference case).

4.3 Sensitivity analysis

In the framework of the evaluation of the effect of different uncertainties and the amount of available data, within INSIDER WP6, a series of modifications were made to the probabilistic reference case outlined in Section 4.2.2. For all these modifications, except the deterministic case,

we created 100 realizations of the 3D grid with Ba-133, Co-60 and Eu-152 activities, and corresponding sum formula outcomes. The estimations are independent from the location of the individual voxels. To illustrate the results of this exercise, we decided to focus on the following:

i. The **volume of concrete** categorized as conditional release, based on the final minimum sum formula result.
ii. The **total activity** in the volume corresponding to the unconditional release.
iii. The **maximum block activity concentration** based on the centred block averages.

4.3.1 Effects of different uncertainties

We considered the following set of modifications to the reference case, to illustrate the effects of the different uncertainties:

i. **deterministic**: The deterministic case corresponds to the reference case with all uncertainties turned off,
ii. **no-measurement-uncertainty**: Corresponds to the reference case without perturbation of the measurement results with 5 and/or 10% random or systematic errors,
iii. **vgm-uncertainty**: Corresponds to the reference case with additionally included perturbation of the fitted variogram models (see Section 4.2.2 for the details),
iv. **no-como-to-ba133-uncertainty**: Corresponds to the reference case without uncertainties of the linear model that converts the COMO cps into Ba-133 activity concentrations,
v. **no-ba133-trend-uncertainty**: Corresponds to the reference case without uncertainties of the linear regression model that captures the main spatial trend,
vi. **no-spatial-uncertainty**: Corresponds to the reference case with deterministic spatial estimation for the Ba-133, Co-60 and Eu-152 residuals rather than geostatistical simulation.

The results of post-processing the different cases are displayed in Figure 30, Figure 31 and Figure 32. Figure 30 illustrates that the volume of concrete labelled as conditional release amounts to roughly between 70 and 100 m³ for the reference case. Most of the other evaluated cases exhibit similar results, although the maximum values may reach up to ~110 m³. For the cases where no corrections for heteroscedasticity are applied (no-fix-heteroscedasticity), or the deterministic spatial estimate is used instead of geostatistical simulation (no-spatial-uncertainty), we get systematically lower volumes however (also note the median of the latter is very close to the deterministic estimate). Although the results are very similar, there are very different reasons behind: Underestimation of the activity concentration residual uncertainty, for values near the thresholds on the one hand, and a lack of spatial fluctuations around the node mean according to the actual spatial correlation on the other. The reason for the lower estimated volume based on the deterministic case compared to the 50th percentile of the best estimate is the effect of the spatial uncertainty that is missing in the deterministic case.

Figure 31 illustrates further that the total activity in the volume labelled as unconditional release changes in a rather minor way between the different evaluated cases, except for the case where a deterministic spatial estimate is used for the residuals (no-spatial-uncertainty), which is more in line with the fully deterministic case.

The maximum block activity concentrations displayed in Figure 32 suggest this outcome is also rather robust with respect to the different uncertainties. The only pronounced changes are observed when we do not account for the heteroscedasticity (no-fix-heteroscedasticity), or we consider deterministic spatial estimation for the residuals (no-spatial-uncertainty). This is however according to our expectations. The Ba-133 trend model error is overestimated for the larger activity concentrations due to the presence of heteroscedasticity, which is directly translated to increased

maximum block activity concentrations. Furthermore, the deterministic spatial estimation for the residuals gives us a best estimate on a node by node basis, which results in an overly smooth outcome, without any fluctuations around that best estimate based on the actual data-based spatial correlation. Since this is done after log transformation, we get systematically lower values for the activity concentrations and corresponding sums compared to the reference case, where we do have those fluctuations around the mean, and the values above the mean have much bigger impact in the arithmetic block averages than those below because of the log scale.

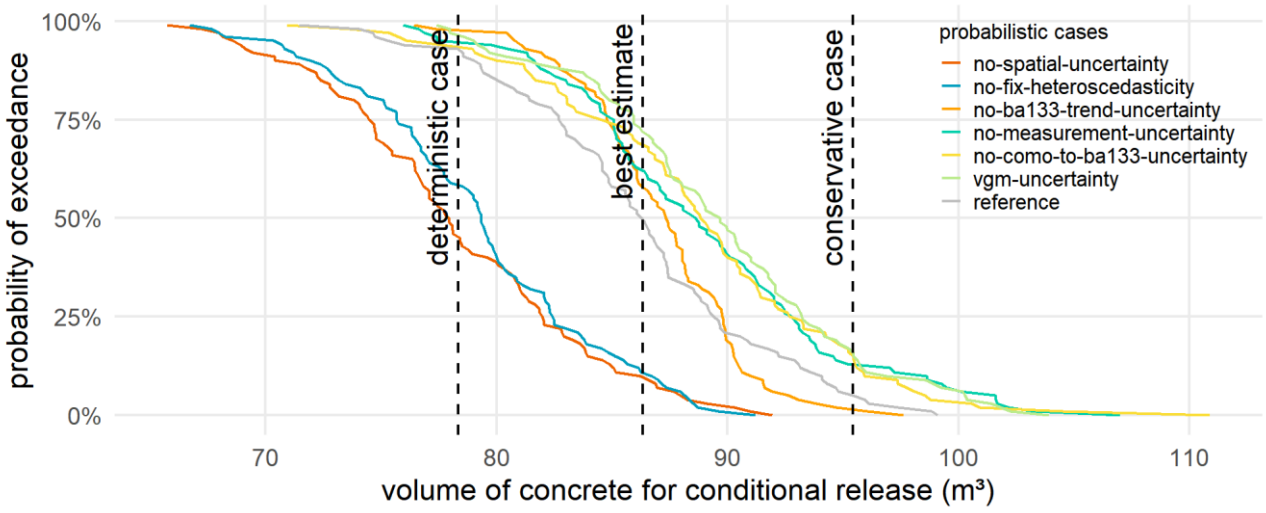

Figure 30: Complementary cumulative distribution function for the volume categorized as conditional release, in function of the different cases with respect to uncertainties.

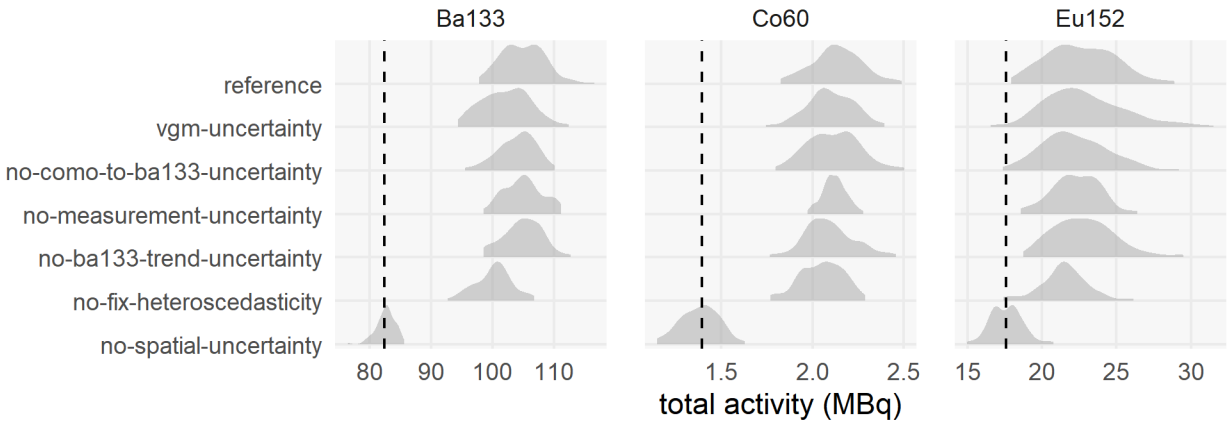

Figure 31: Total activity distributions for the different isotopes, over the volume corresponding to the unconditional release category, in function of the different cases with respect to uncertainties. The dashed line represents the deterministic case.

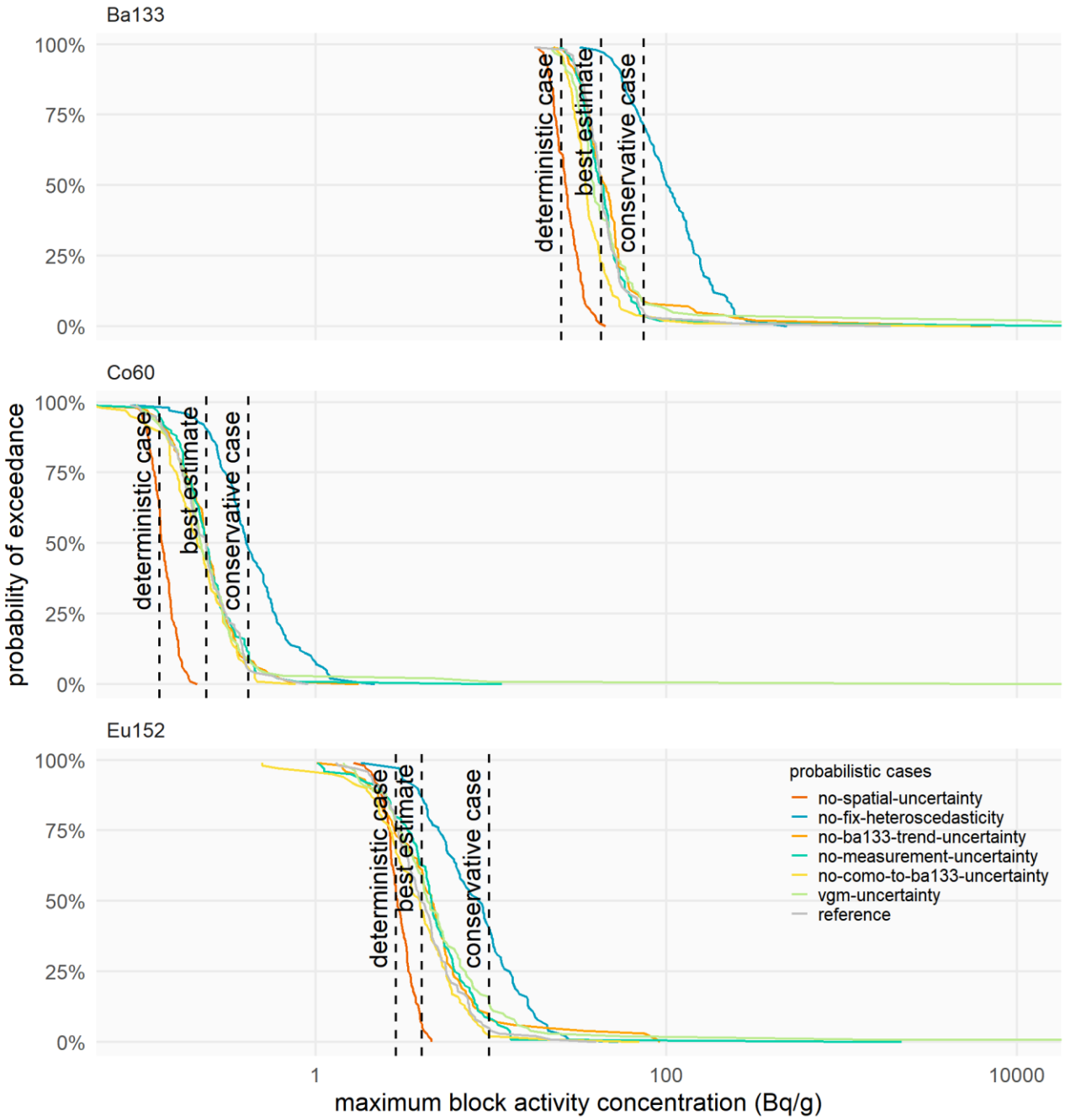

Figure 32: Complementary cumulative distribution function for the maximum block activity concentrations, for each of the three isotopes, in function of the different cases with respect to uncertainties.

The conclusions for the end user in terms of the effects of different uncertainties on the volume categorized as conditional release are the following:

- The final data set consists of 834 data points (415 primary and 419 secondary), which comes down to more than 1 data point per m^3.
- The global uncertainty of 13% (50->95 for the reference case) is more than satisfactory.
- The most important uncertainties are related to the heteroscedasticity and the geostatistical simulations.

- Uncertainties due to the measurements uncertainties on primary and secondary data, the transformation from Como data to Ba-133 activity concentration and the Ba-133 trend model are relatively limited.

4.3.2 Effects of reduced amounts of data

We considered the following set of modifications to the reference case, to illustrate the effects of different data amounts and types:

i. **no-como-samples**: Corresponds to the reference case without the secondary total gamma COMO dataset,
ii. **only-15-boreholes**: Corresponds to the reference case, including secondary total gamma COMO data, but the number of boreholes with primary data is reduced to 15 (*i.e.* 100 primary data points remain; see Figure 33),
iii. **only-15-boreholes-without-como**: Corresponds to the reference case using only the reduced set of 15 boreholes (no secondary total gamma COMO data included).

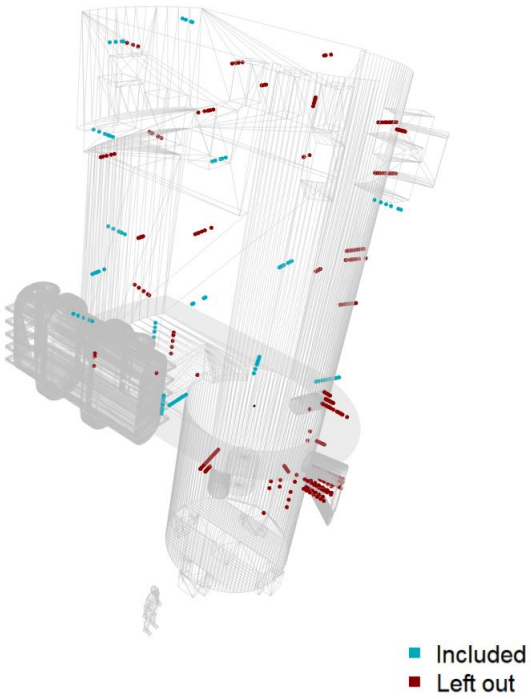

Figure 33: Indication on which borehole samples are included in the reduced set of 15 boreholes, and which are left out.

The results of post-processing the data amount/type cases are displayed in Figure 34, Figure 35 and Figure 36. Figure 34 indicates that with less borehole data, or no secondary data, we seem to get a systematic drop in the volume categorized as conditional release, while the uncertainty remains more or less constant. For the minimal data case, without secondary data and only 15 boreholes, the uncertainty clearly inflates from a range of about 30 m³ to more than 120 m³. Also, comparing the case without secondary data with the reference, seems to indicate we would end up

with quite some underestimation of the volume, while for the reduced number of boreholes, we would still cover the reference case range because of a tail towards the larger volumes.

The total activity in the volume categorized as unconditional release also shows clearly larger uncertainty for Ba-133 in case of the minimum amount of data (reduced set of boreholes and no secondary data) in Figure 35. For Co-60 and Eu-152, the pattern looks different, however, as the reduced set of boreholes seems to lead there to lower total activities, and also a bit less uncertainty in case of Eu-152. This is a consequence of the borehole subset influencing the linear model fit for the scaling factor approaches, at least for the gray concrete type in case of Eu-152, and the lower activity concentrations for Co-60 (see also dashed lines in Figure 23). In terms of total Co-60 and Eu-152 activities for the volume categorized as unconditional release, this results in the reference case being the most conservative however.

Figure 36 suggests that only the minimum data case (15 boreholes and no secondary data) results in considerably larger maximum block activities for all isotopes. For the case without secondary data, the estimates are systematically larger than for the reference as well.

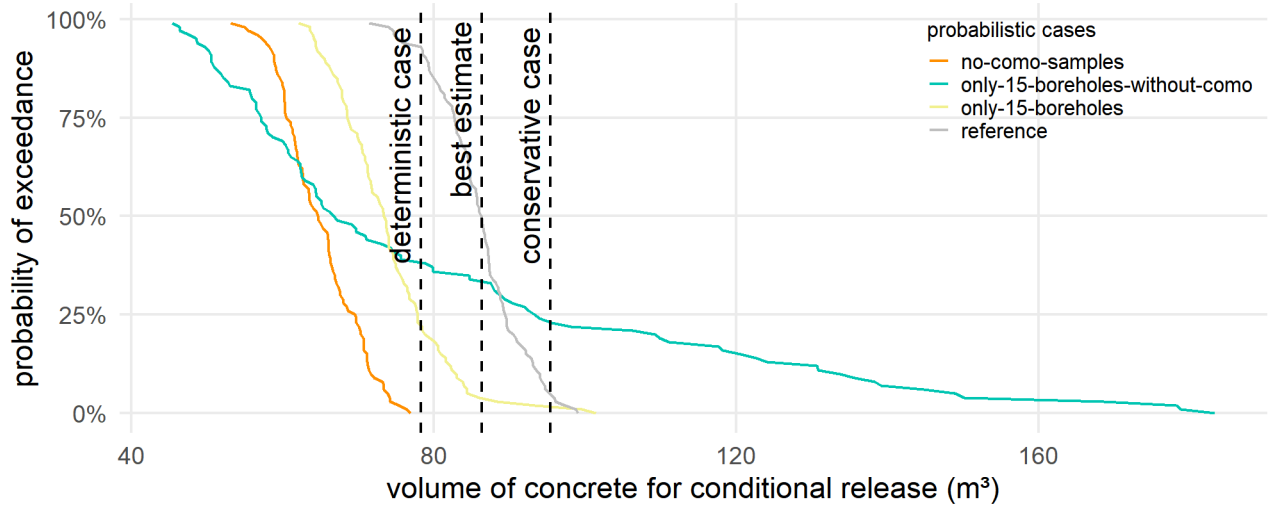

Figure 34: Complementary cumulative distribution function for the volume categorized as conditional release, in function of the different cases with respect to data amounts/types.

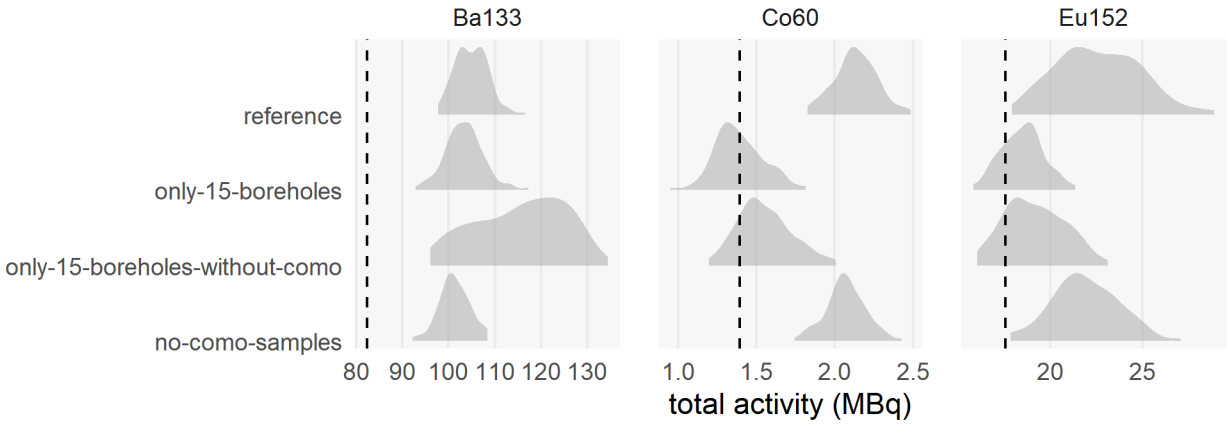

Figure 35: Total activity distributions for the different isotopes, over the volume corresponding to the unconditional release category, in function of the different cases with respect to data amounts/types. The dashed line represents the deterministic case.

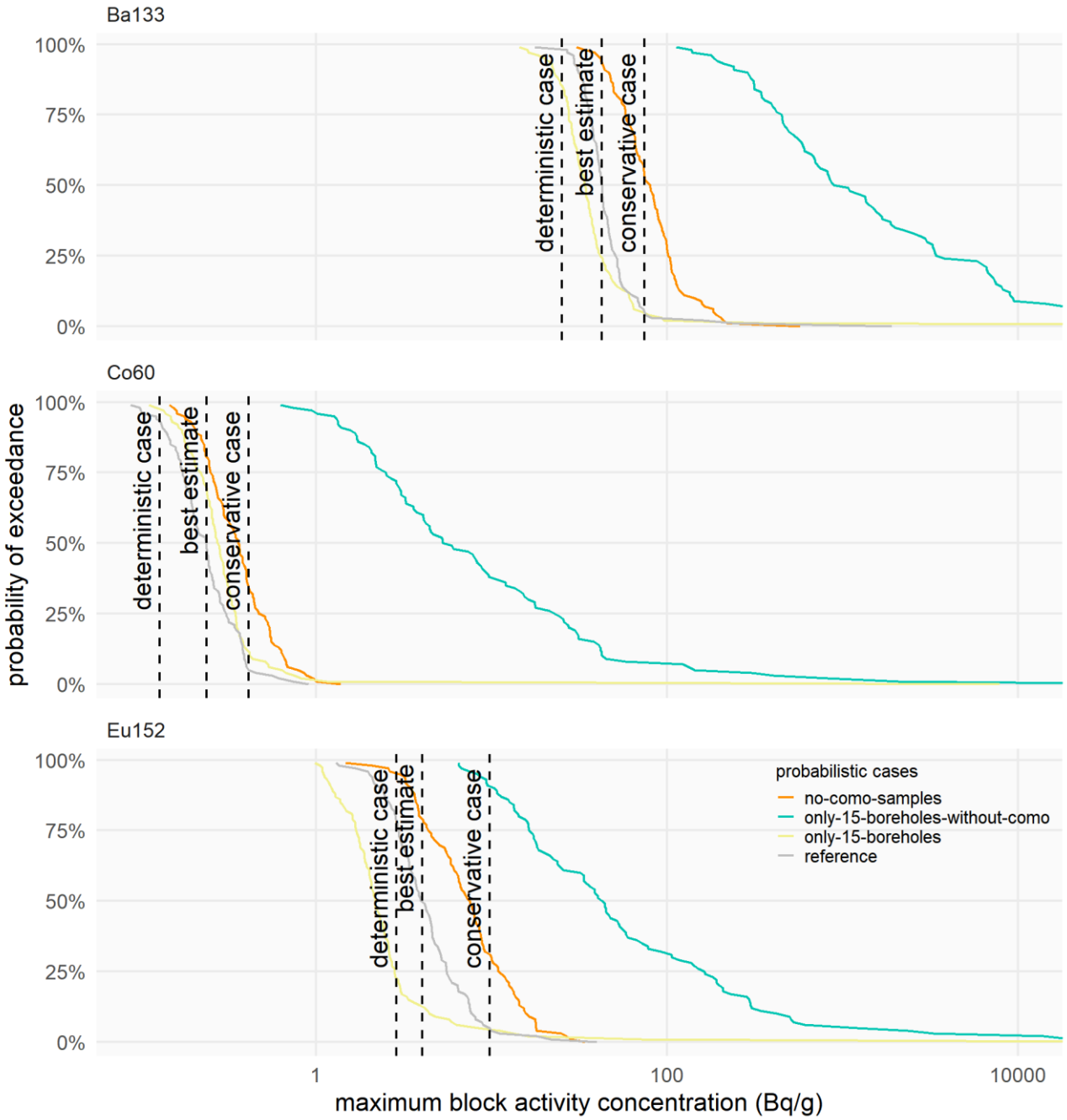

Figure 36: Complementary cumulative distribution function for the maximum block activity concentrations, for each of the three isotopes, in function of the different cases with respect to data amounts/types.

The conclusions for the end user in terms of the effects of reducing the amount of data on the volume categorized as conditional release are the following:

- Removing the (secondary) Como data has a very limited effect on the total activity calculation for the unconditional release category. It might however lead to an underestimation of the volume categorized as conditional release of about 25%. This might be mainly a result of an underestimation of the volume around NST.
- Reducing the primary dataset down to 15 boreholes (a reduction of 75% of the data points):

- Only results in a limited underestimation of the volume of concrete for unconditional release (about 15%) in the case where the secondary Como data are included in the data set.
- Could result in extreme under/over estimation of the volume of concrete for unconditional release when no secondary data are available.

4.3.3 Cross-validation

As we evaluated two cases within the sensitivity analysis, where only 15 boreholes were used, we have the possibility to look at the probabilistic model performance in terms of the boreholes left out, to get an idea on its adequacy. Figure 37, Figure 38 and Figure 39 illustrate the logarithmic Ba-133 activity concentration profiles in the wall for all boreholes, with an indication of those not used in the model, and hence useful for cross-validation (*i.e.* in Figure 38 and Figure 39), while Figure 40 provides an overview of where the points exceeding the 95th percentile are located in 3D.

Figure 38 does reveal that in case of a reduced number of boreholes, most of the validation data points fall within the probabilistic model ranges. There are only a handful of large outliers, and most deviations are concentrated at the NST pit, more specifically around the hot/cold legs, as also revealed by Figure 40b. As the reduced set of 15 boreholes does not include any of the boreholes around the known anomaly near the hot/cold legs, this was to be expected and hence does not invalidate the model.

In the minimum data case, illustrated in Figure 39, most of the results above the reactor pool floor are in fact still in accordance with the model. We do get large overestimation of the activity concentrations in the NST pit and near the hot/cold legs however, especially near the inner surface of the wall. This results in much less underestimation by the model, comparable with the reference case (Figure 40a and c).

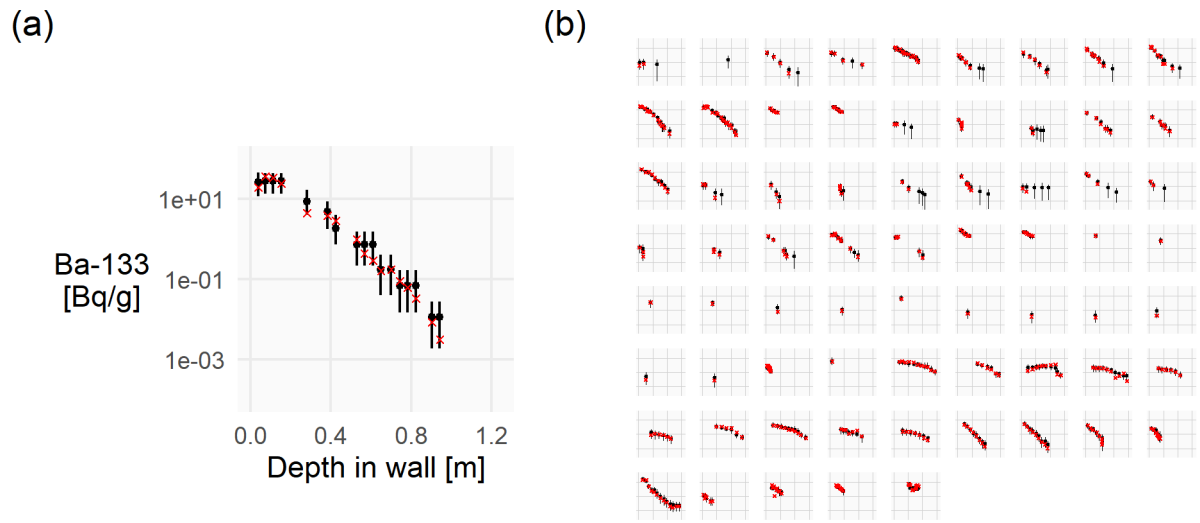

Figure 37: Reference case median and 95% interval (black) versus observed (red) Ba-133 activity concentrations: Example borehole (a), part of the reduced set of 15, and overview of all boreholes (b).

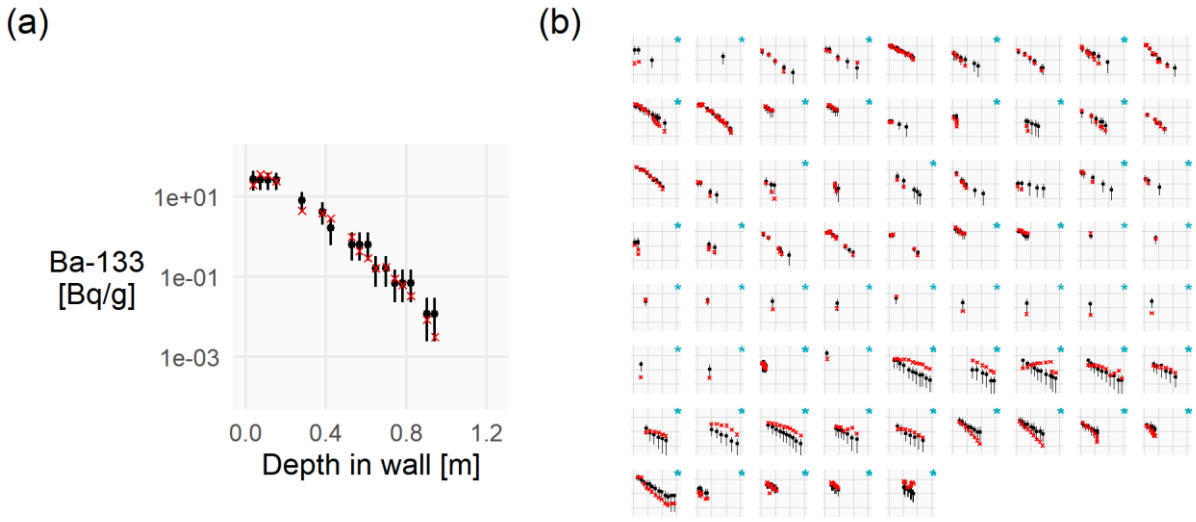

Figure 38: Reduced primary data case (15 boreholes and secondary data) median and 95% interval (black) versus observed (red) Ba-133 activity concentrations: Example borehole (a), part of the reduced set of 15, and overview of all boreholes (b), with asterisks indicating boreholes for cross-validation.

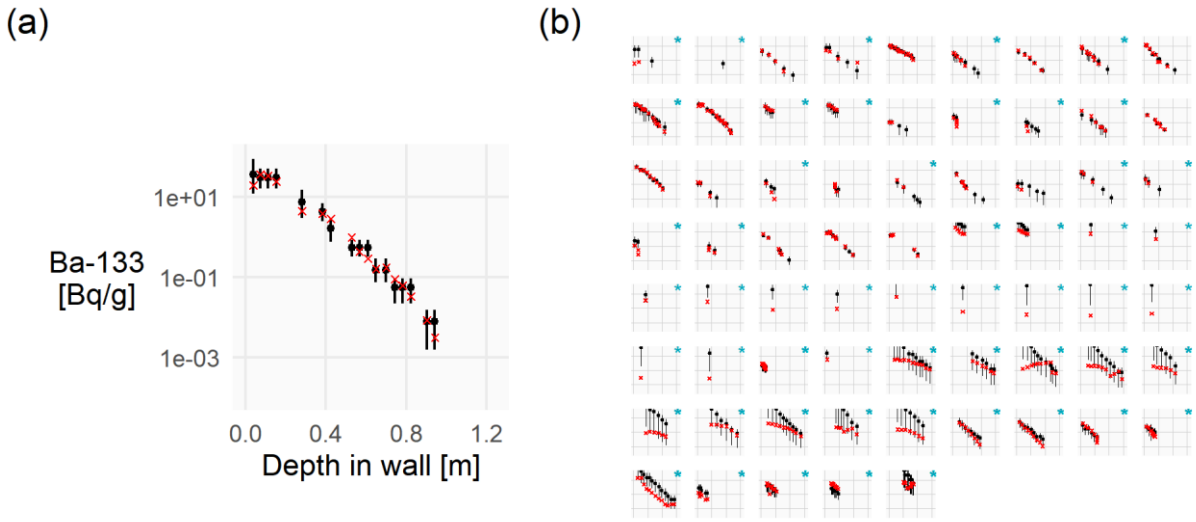

Figure 39: Minimum data case (only 15 boreholes) median and 95% interval (black) versus observed (red) Ba-133 activity concentrations: Example borehole (a), part of the reduced set of 15, and overview of all boreholes (b), with asterisks indicating boreholes for cross-validation.

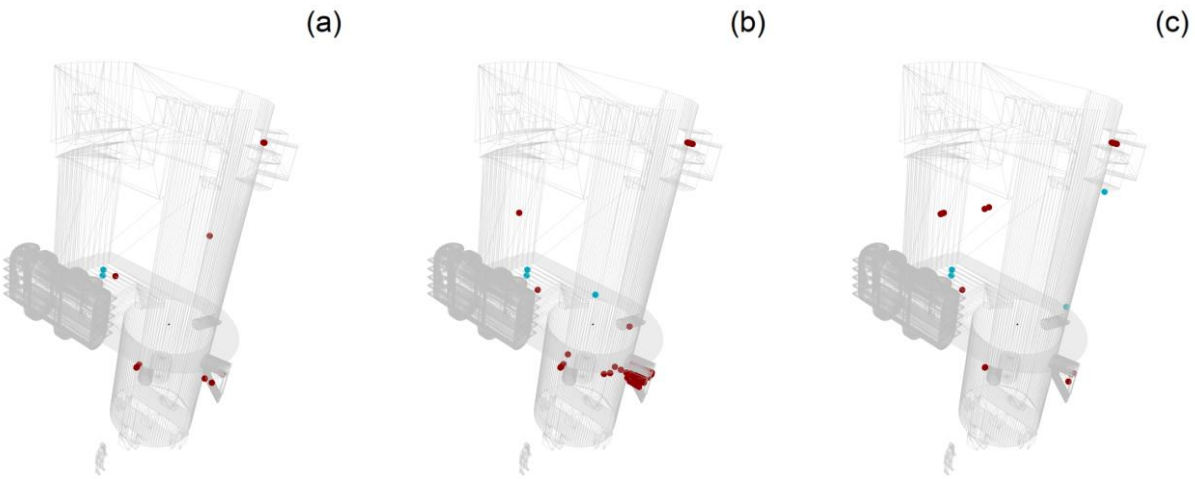

Figure 40: Overview of the Ba-133 activity concentration data points beyond the 95th percentile of the model (*i.e.* where the model underestimates activation levels), in the reference case (a), the reduced primary data case (b), and the minimum data case (c). The Figure 33 colour scale is used to indicate the samples included and those left out in the model, for subfigures (b) and (c).

Table 5 provides an overview of the percentages of validation data points beyond the 5th and 95th percentiles. Where we expect these to be around 5%, it should be noted here the results are only based on 100 simulations, which may result in significant fluctuations around 5%, even if the model would be perfect. For the reference case, these samples are included in the model, and hence no issues are to be expected (as apparent from the table). For the reduced set of 15 boreholes we do get considerable underestimation, even more for Eu-152 than for Ba-133 it seems. As mentioned above, this is mainly due to the exclusion of the data around the hot/cold legs, and for Eu-152 likely also due to changes in the scaling factor model fit. For the minimum data case, with only 15 boreholes and without any secondary data, the uncertainties inflate at the NST pit and around the hot/cold legs, which results in very little remaining underestimation (except for Eu-152), while we do have considerable overestimation in this case (which is judged less important as the model is conservative in this case).

Table 5: Overview of the percentage of validation data points (not included in reduced set of 15 boreholes) beyond the 5th and 95th percentiles of the reference case and the cases with a reduced number of boreholes. Cells where the expected 5% is exceeded are highlighted.

	Percentage of points	
	< 5th percentile	> 95th percentile
Case: reference		
Ba133	1.05%	1.40%
Co60	0.00%	3.14%
Eu152	0.47%	1.41%
Case: only-15-boreholes		
Ba133	7.02%	20.00%
Co60	1.89%	16.98%
Eu152	4.23%	44.13%
Case: only-15-boreholes-without-como		
Ba133	16.14%	4.91%
Co60	15.72%	1.89%
Eu152	8.45%	9.86%

4.4 Objectives achieved

The main goal was to economically optimize the biological shield dismantling strategy using a waste-led approach. In order to reach this main goal, three objectives were defined (see Section 1.2), which were achieved as follows:

1. Create a sufficiently reliable 3D activity concentration distribution model, that includes uncertainty estimates:
    a. The used dataset covers as much as possible all extremes, to avoid extrapolation as much as possible, as discussed in Section 2.4,
    b. The 3D activity concentration distribution model is outlined in Section 4.2.1,
    c. How uncertainties were included is outlined in Section 4.2.2,
    d. A cross-validation for assessing the reliability is discussed in Section 4.3.3,
    e. All remaining issues with the model are related to known local anomalies, and hence good argumentation is available to locally depart from the model outcome if required,
2. Economically optimise volumes in view of a waste-led approach taking unconditional and conditional release end stage options into account:
    a. The effect of considering block averages is studied in detail, and the most optimal solution within the constraints is used in the end,
3. Quantify and localise the different end-stage volumes:
    a. An illustration of the horizontal slice exports is discussed in Section 4.2.4,
    b. The volume labelled as conditional release, and its uncertainty, is discussed in Section 4.3.

4.5 Reporting results

During the various stages of the sampling design, characterization and data analysis process, we organized intermediate meetings with the end user discussing the progress and assessing the achievement of the objectives together. On the one hand, it is important that the end user fully understands the assumptions that have been made. On the other hand, the characterization and data analysis experts need to perceive the consequences of the results on the further segregation strategy and its limitations. These regular interactions are indispensable to reach effective results. In order to prepare for the strategy and the regulatory documents, the reported output consisted of two series of PDF exports horizontal slices for every 0.1 m through the biological shield grid: one for the best estimate (median) and one for the conservative estimate (95^{th} percentile). The latter is being used by the dismantling experts to define the segregation strategy.

5 Supplementary quality control measures

Related to the measurement data quality, the INSIDER project provided several types of comparison/benchmarking exercises:

- On-site intercomparison exercise to compare various types of in-situ measurement results obtained by various measurement teams at pre-defined locations in the BR3 biological shield (see Figure 41a).
- In-lab intercomparison exercises:
  - an interlaboratory comparison exercise on reference material (RM) and
  - a benchmarking exercise on real samples (see Figure 41b).

Furthermore, related more to the 3D model quality, and in view of defining the dismantling and material separation strategy, the SCK CEN performed a concrete separation test, during which we performed several control measurements.

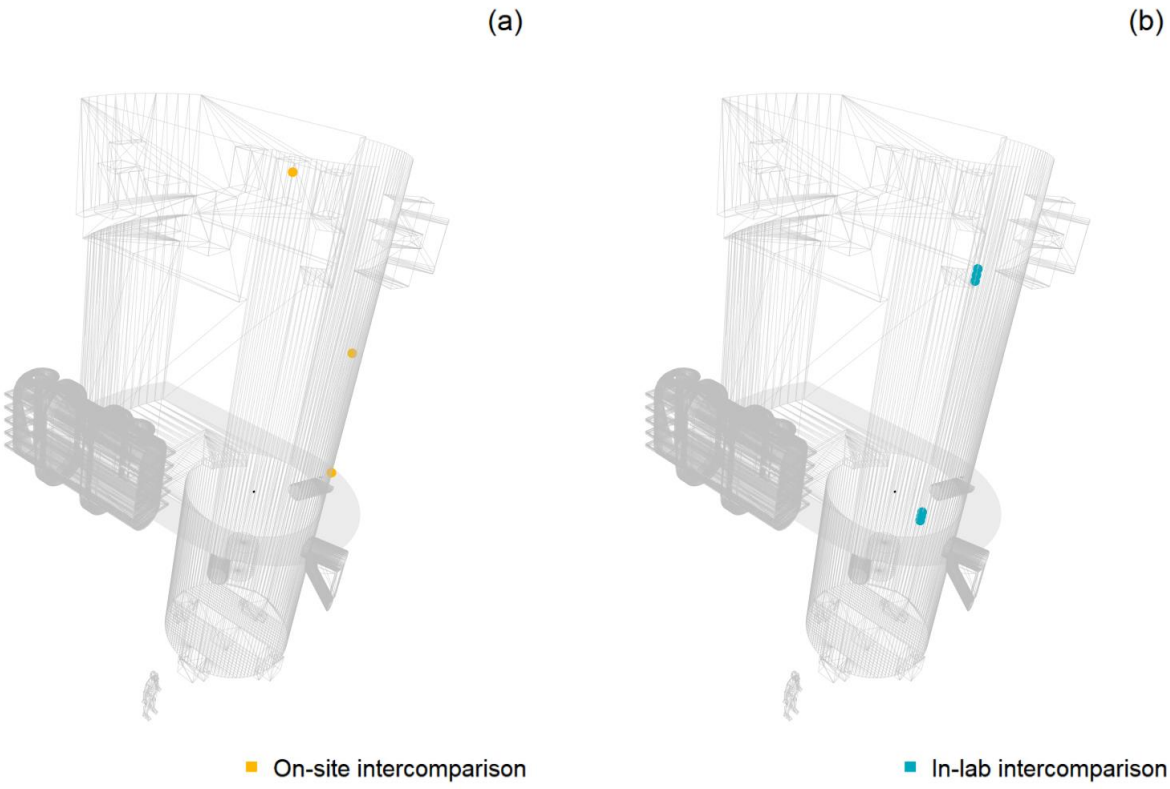

Figure 41: Overview of the on-site intercomparison exercise locations (a), and the sample locations for the in-lab intercomparison (b).

5.1 UC2 on-site intercomparison exercise

The UC2 benchmarking exercise has been accomplished during the last quarter of 2018, by performing various radiological measurements in the biological shield of the BR3 reactor. The exercise and results are extensively described in separate documents (Herranz, et al., 2021). This section only summarizes the setup of this exercise and the results that are important for the BR3 biological shield model.

Seven measurement teams from the following seven different organisations participated to the UC2 on-site benchmarking exercise (alphabetical order):

- KIT, Karlsruhe Institute of Technology (Germany)
- Mirion Technologies (France)
- MTA-EK, Hungarian Academy of Sciences Centre for Energy Research (Hungary)
- PSI, Paul Scherrer Institute (Switzerland)
- SCK•CEN, Belgian Nuclear Research Centre (Belgium)
- Tecnatom (Spain)
- UPV/EHU, University of the Basque Country (Spain)

As a starting point for the UC2 on-site benchmarking exercise, we considered two types of relatively simple, commonly used, fast, easy and straightforward measurement methods: dose rate and total gamma. Additionally we examined the feasibility to use in-situ gamma spectrometry in this stage of the characterisation process. In order to **cover the full range of activity concentration levels** for the biological shield, we selected **three fixed points** to perform dose rate and total gamma measurements (see Figure 41a):

- Point A, at the top of the reactor pool (relatively low activation levels),
- Point B, approximately in the middle at medium height in the reactor pool (medium activation levels), and
- Point C, close to the bottom of the reactor pool and therefore close to the maximum activation levels.

The dataset used for reaching the characterization objectives for the BR3 biological shield does not contain any dose rate nor in-situ gamma spectrometry measurements. It solely contains total gamma measurement results (mainly Como 300G and a few CZT) used as in-situ secondary data (see section 4.1). Consequently, this section does not contain the results from the dose rate nor from the in-situ gamma spectrometry intercomparison exercise. Instead, we concentrate on the **total gamma measurement results**. Table 6 shows the equipment used by the various participants for performing the total gamma measurements.

Table 6: Overview of the equipment properties used by the participants for the total gamma measurements

Detector principle	Proportional counter		Scintillator					
Detector type	Gas	Gas	ZnS	ZnS + organic	Organic	NaI(Tl)	$LaBr_3$	BGO
Brand	Berthold	Thermo Scientific	Berthold	NuviaTECH instruments	NuviaTECH instruments	Mirion	Mirion +Hamamatsu	Own design
Model	LB 1236	FH40 G-L10	LB124	Como 170	Como300G	SG2R	$LaBr_3$ 1,5 “	/
Detector shape	cylindrical	cylindrical	rectangular	rectangular	rectangular	cylindrical	cylindrical	Cylindrical
Size (cm)	3.4 X 11	2.5 × 2.58	24 x 14.2 x 1.1?	24 x 13 x 0.1	24 x 13 x 2	5.08 x 5.08	3.81x3.81	1.485 x 0.8
Surface (cm^2)	9.1	39.9	341.0	312.0	312.0	20.3	11.4	1.7
Volume (cm^3)	99.9	25.3	34.5	31.2	624.0	103.0	43.4	1.4

The total gamma measurements are used as secondary data within the data analysis process. This means that only the relative values are important for the radiological characterization process. Trueness and reference values are trivial, so we do not need to account for systematic errors here.

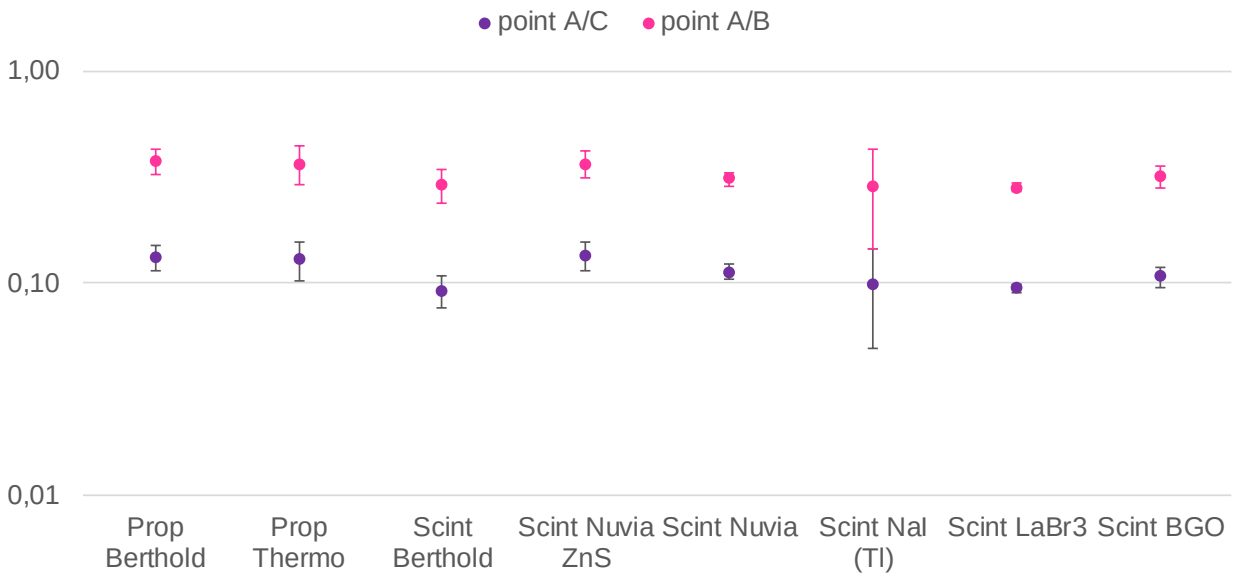

Figure 42 presents the total gamma ratios point A/point C and point A/point B for the various detectors. The proportional counters seem to give larger values (potentially due to an effect of beta radiation or low energy photons). The $LaBr_3$ detector results represent the lowest uncertainty, followed by the Organic Nuvia detector with 20 mm thick crystal. The Organic Nuvia detector Como 300G is the detector used by SCK CEN for mapping of the inner surface of the biological shield in view of reaching the UC2 goal. Figure 43 shows the measurements results of the Como300G during the UC2 on-site intercomparison exercise Five sets consisting of five consecutive measurements each (in order to test repeatability), were carried out for each of the three points. Between every set, the equipment was removed and repositioned (in order to test reproducibility). This resulted in a total of 25 single total gamma measurements for each point. Using this detector applying a 30 s integration time results in an **expanded uncertainty for the repeatability and reproducibility between 3.4% and 6.5%**. Hence, for the random component of the error of the COMO 300G dataset used for the development of the 3D model of the bioshield, we considered an expanded uncertainty (coverage factor 2) of 5% during the simulations described in Section 4.

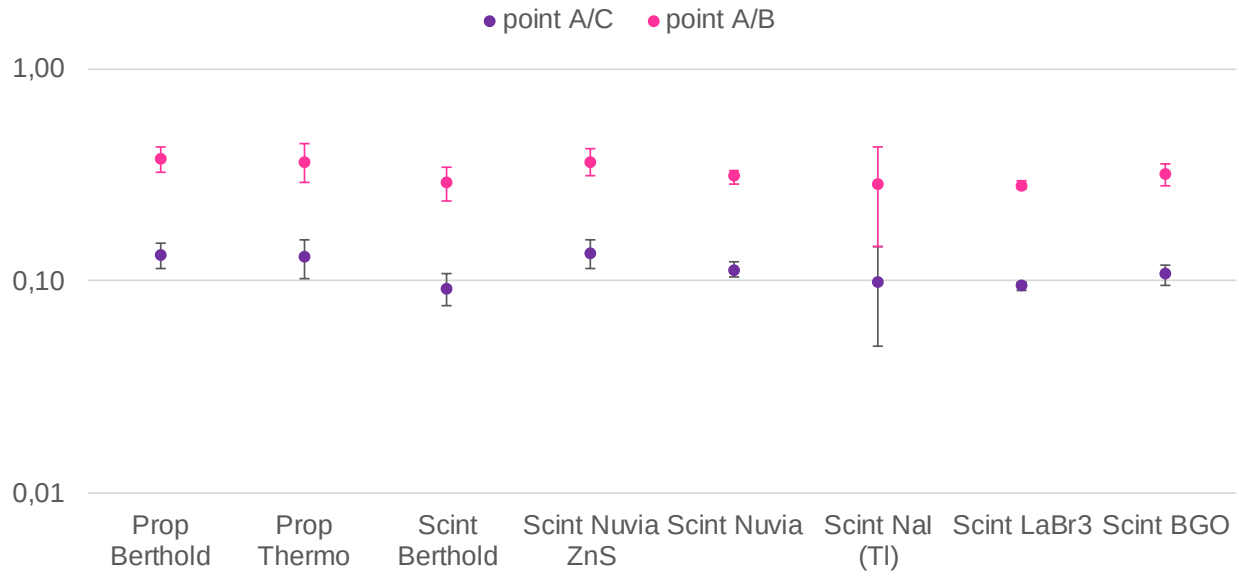

Figure 42: Total gamma ratios (logarithmic scale) for points A/C and points A/B for the various detectors used. The error bars represent the expanded uncertainty (coverage factor 2)

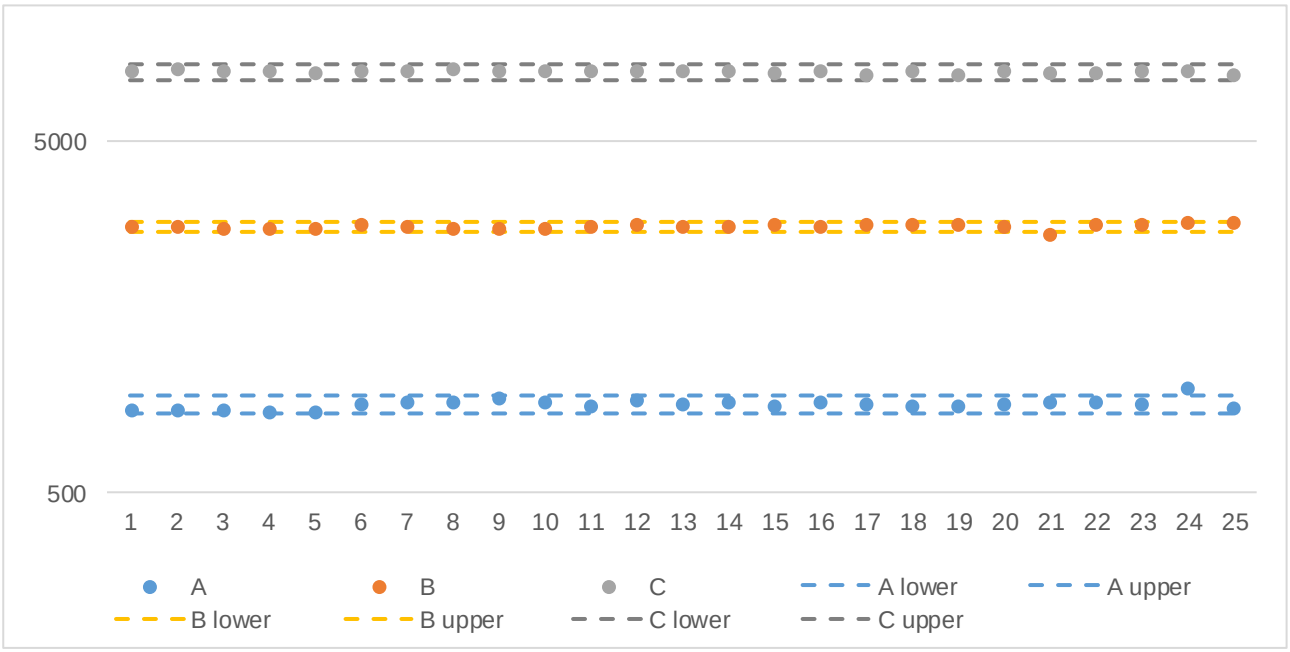

Figure 43: Como 300G count rates (cps, logarithmic scale) for 25 measurements of point A, B and C (dots). The upper and lower limits at 95% confidence level are indicated with dotted lines.

5.2 UC2 in-lab intercomparison exercise

During the sampling campaign (see chapter 3), additional concrete samples at two different locations were taken (see Figure 41b) and provided to the National Physical Laboratory (NPL). NPL took care of the homogenization and distribution of sub-samples to various EU labs belonging to the INSIDER consortium in view of performing a benchmarking exercise within the INSIDER project. The SCK CEN also provided inactive concrete for the production of reference samples and organization of an interlaboratory comparison. The detailed set-up of the exercises and its results are described in (Crozet, Demeyer, Lourenco, & Rivier, to be submitted). This report only briefly describes the results of the gamma spectrometry.

The sample geometry consisted of a 50 ml powder geometry, which was different from the disc geometry used for the real data of the biological shield. Comparisons in laboratory consisted of a Certified Reference Material (CRM) concrete made of non-irradiated heavy concrete from BR3 and two real representative samples from the BR3 activated biological shield: a sample with a Ba-133 activity concentration in the range of 10 Bq/g and a sample with a Ba-133 activity concentration in the range of 3 Bq/g. The results of this exercise, relevant for the UC2 uncertainty budget, can be summarized as follows:

- Unfortunately, the radionuclide composition of the CRM concrete was not representative for the BR3 biological shield, due to its different geometry (50 ml powder instead of disc) and the radiological composition. The CRM contained a relatively high amount of Co-60 with high energy photons, compared to a low amount of Ba-133 with low energy photons. In the BR3 biological shield, we have the opposite situation: a relatively high amount for Ba-133 and a relatively low amount for Co-60. For the CRM, the artificial radionuclide composition resulted in an estimated measurement uncertainty (k=1) of 32% for Ba-133, 12% for Eu-152 and 5.2% for Co-60. In any case, the bias of the gamma spectrometry method was not significant (the normalized deviation calculated for each of the radionuclides is less than 2 in absolute value).
- The reproducibility (k=1) for the two real samples was the following (from higher to lower Ba-133 activity concentration): 5.7-9.0% for Ba-133, 8.5-11% for Eu-152 and 6.8%-8.9% for Co-60.

During the development of the BR3 biological shield model, we did not yet have the results of the interlaboratory exercise. At that time, we therefore decided to perturb the primary data with a systematic error of 10% and a random error of 10% (k= 2), for each isotope separately and independently from the activity concentration (see Section 4). In retrospect, this is not fully correct and could be optimized by using results from the interlaboratory comparison, but sufficiently representative.

5.3 Control measurements during concrete separation tests

The SCK CEN D&D unit performed tests to in-situ remove the part of the concrete requiring conditional release, from the remaining concrete eligible for unconditional release. For the separation, we applied remote controlled pneumatic hammering. The test section consisted of a part of wall 087-03, from the reactor pool floor (z = 0) up to 2 m height, over the entire wall length.
After removal of a concrete layer to a depth of about 50 cm in the test section, we collected samples at 12 different locations. Each sample contains concrete dust collected from drilling a 300 mm deep hole (35 mm diameter) using a widia drill. Figure 44 shows the location of the samples:

- 8 horizontal samples (087-03-12 up to 19) in the green zone, pointing towards the outside of the reactor building at two different heights (z=0.436 and z=1.436).
- 2 horizontal samples (left: 087-03-08 in the neighbourhood of the former “poubelle” and right: 087-03-11) in the corners of the walls, mainly in the blue (transition) zone (z=0.936).
- 2 vertical samples (left: 087-03-09 in the neighbourhood of the former “poubelle” and right: 87-03-10), mainly in the blue zone (left) and in the orange zone (right).

The collected dust was analyzed in the lab using high-resolution gamma spectrometry. Figure 45 shows the sum formula calculation for the sample measurements and a comparison with the reference case sum formulas at the point scale. The red line represents the transition between unconditional and conditional release. We notice the following:

- For the 8 horizontal samples located in the green zone (087-03-12 up to 19): Sample measurement results are very clearly below the limit for unconditional release.
- For the 3 samples mainly located in the transition zone (087-03-08, 087-03-11 and 087-03-09): the sample measurement results are below the limit for unconditional release, while according to the model it could exceed.
- For the 1 sample located in the orange zone (087-03-10): both sample measurement result and value according to the model are clearly above the limit for unconditional release.

The agreement between the results of the control measurements and the model is good, taking the grid size (10 x10x10 cm) into account. Some asymmetry exists between the left and right hand part of the outside wall as discussed in 4.2.1 and this is probably more pronounced than the model suggests. During reactor operation the left side of the outer wall was shielded by a lead structure ("poubelle") which was used to store reactor-internals. The structure itself was already dismantled in 2003 and was not included as such in the model. Nonetheless, the conservative case model (95th percentile) is sufficiently conservative without being too conservative for developing the concrete separation plan.

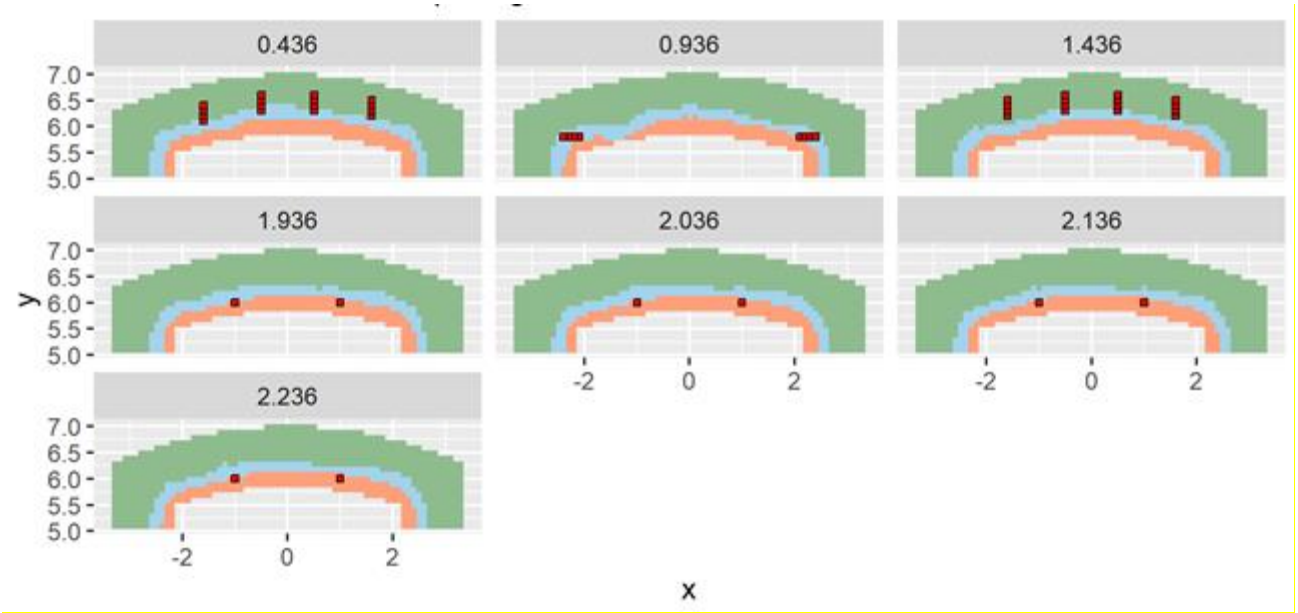

Figure 44: Horizontal cross sections of the test area of wall 087-03 (different z-values between z=0m and +2m), indicating the region fulfilling the criteria for unconditional release according to the 95th percentile (green) and conditional release according to the 50th percentile (orange). The transition zone in between (blue) corresponds to the safety factor. Eight samples have been mainly taken in the green zone (z=0.436 and 1.436). The four remaining samples, two horizontal cores (0.936) and 2 vertical cores (z=1.936 up to 2.236) have been taken in the orange (partly blue) zone.

Figure 45: Calculated sum formula for unconditional release: comparison of sample measurement results and the corresponding 50th percentile for the sample voxels (without averaging). The red line indicates the transition between conditional and unconditional release.

6 UC2 lessons learnt

UC2 shows how the data analysis and sampling design strategy has been implemented for the initial radiological characterization of the biological shield of the Belgian Reactor 3. The implementation consisted of three stages: a preliminary data analysis based on pre-existing data & sampling design (stage 1), the execution of the sampling plan, data analysis on the combined dataset & post-processing (stage 2) and the additional data gathering & data analysis on the final dataset (stage 3). The predefined strategy was carefully followed, leading to highly reliable and fit for purpose results. We further list the lessons learnt in terms of the overall strategy, data analysis and sampling design approach and specific aspects regarding uncertainties.

6.1 Overall strategy

Very **clear and quantifiable objectives** were defined for UC2 prior to start the exercise. This allowed the development of an effective sampling plan including the selection of appropriate measurement techniques and the up-front definition of criteria for the measurements (e.g. detection limits, uncertainties). Nevertheless, the Belgian regulation changed during the execution, resulting in a modification of the objectives. Fortunately, this change did not impact the sampling strategy nor the decision threshold between unconditional and conditional release.

Detection limits were typically more than ten times below the decision criterion and samples were carefully selected. Consequently, there were only very few results below the detection limit. The few results below detection limit (7% out of the 415 primary data points for Ba-133) have been discarded with negligible impact on the quality and size of the data set.

Decommissioning is a **multi-disciplinary operation**. The involvement of specialized staff performing the next stages of the decommissioning project has proved to be beneficial. Technical feasibilities/constraints in the next stages might strongly influence the initial characterization program. The use of 3D models and detailed 2D PDF exports of all horizontal slices through the biological shield grid has significantly improved common understanding and enhanced decision taking.

6.2 Data analysis and sampling design strategy

Obviously, a problem with extrapolation impacted the characterization process (at stage 2) and planning. **Extrapolation should be avoided at all times**. This does not only concerns the expected activity concentrations (lowest and highest), but as well the physical location. It is obvious that in a certain stage in the dismantling process, it might be difficult or impossible to reach the extremes for performing in-situ measurements or for taking samples. In this case, it is necessary to foresee the measurements at a later stage in the project and to update the existing data analysis and post processing. Just ignoring the information might result in unacceptable uncertainties. Nevertheless, performing a radiological characterization program in two or three **stages** can be efficient and effective to tackle areas with higher uncertainties. Historical data, sometimes gathered with other objectives (e.g. analysis liner samples) can optimize the characterization process.

The draft guideline foresees some quality assurance checks (e.g. errors, outliers, sample representativeness) on the existing data during the pre-processing step. However, the current version does not mention any **validation techniques** for assessing the results obtained. This aspect should be incorporated in the final version.

The current version of the data analysis and sampling design web tool (https://insider-h2020.sckcen.be/), already contains a list of theoretical examples, software implementations, example use cases and references. All **use case annexes** should, together INSIDER WP3 publications, be made available in the tool as well.

6.3 Sensitivities & uncertainties

In the framework of the INSIDER project, it was not foreseen to perform a full analysis of uncertainties and sensitivities. The approach followed consisted of introducing a series of modifications to the probabilistic reference case, followed by **assessing the effects** on the volume of concrete categorized as conditional release, the total activity in the volume corresponding to the unconditional release and the maximum block activity concentration based on the centered block averages. Effects of different uncertainties could be different on volume, total activity and maximum block activity, but are in any case most affected by the spatial uncertainty and heteroscedasticity.

The main UC2 objective is to estimate the **volume categorized as conditional release**. The sensitivity analysis shows here that a global uncertainty of 13% (best estimate compared to 95th percentile) on the volume categorized as conditional release is more than satisfactory. Uncertainties due to the measurements uncertainties on primary and secondary data, the transformation from Como data to Ba-133 activity concentration and the Ba-133 trend model are relatively limited. The most important uncertainties are related to the heteroscedasticity and the geostatistical simulations. Trend models and logarithmic transformations can result in large uncertainties. Accounting for heteroscedasticity effects can be important. An important note is that the estimated volumes for the sensitivity analysis described in this report relate to the volume not complying with the sum formula including averaging over a certain volume/mass. This means that the estimated volumes for the elaborated examples in this document are independent from the location of the volume. For the real licensing file, we followed a different approach, since we require 95% confidence at each spatial location.

Reducing the primary dataset down to 15 boreholes (roughly 1 borehole per 40 cubic meter), could result in extreme under/over estimations of the volume of concrete for unconditional release. The uncertainties can be strongly reduced by combining the limited higher quality and costly primary dataset (in-lab sample measurements) with a large cheap secondary data set (in-situ measurements).

7 Bibliography

Aït Abderrahim, H. (1996). *Assessment of the BR3 concrete building activation using the Tripoli Monte Carlo transport code, Topical meeting on Radiation Protection and Shielding, No Falmouth Massachusetts, USA, Proc. 576-583.* American Nuclear Society.

Aoust, T. (2008). *Evaluation neutronique de l'activation du béton autour du réacteur BR3, Situation 30/04/2008, Internal note.* SCK-CEN.

Boden, S. V. (2018). *Sampling plans for use case 2.* H2020 INSIDER D3.5.

Broeckx, W., Rogiers, B., Mangelschots, N., Vandyck, R., Verstrepen, G., & Boden, S. (2020). INSIDER UC2: the BR3 biological shield preliminary results and future work. *EPJ Nuclear Sci. Technol.*, 6, 14.

Crozet, M., Demeyer, S., Lourenco, V., & Rivier, C. (to be submitted). Interlaboratory comparisons on concretes within the INSIDER project. *Currently unknown*.

Demeulemeester, Y. (2018). *SHEQ - QA manual DDW, SCK-CEN/1259373 Rev. 1.1, DDW-SHEQ-02.* SCK-CEN.

Desnoyers, Y., & Rogiers, B. (2020). Development of a user-friendly guideline for data analysis and sampling design strategy. *EPJ Nuclear Sci. Technol.*, 6, 16.

EURATOM. (2013). *Council Directive 2013/59/EURATOM of 5 December 2013 laying down basic safety standards for protection against the dangers arising from exposure to ionising radiation, and repealing Directives 89/618/Euratom, 90/641/Euratom, 96/29/Euratom, 97/43/Euratom a.* Official Journal of the European Union.

FANC. (2001). *Koninklijk besluit van juli houdend algemeen reglement op de bescherming van de bevolking, van de werknemers en het leefmilieu tegen het gevaar van de ioniserende stralingen (ARBIS).* Belgian Official Gazette.

Herranz, M., Boden, S., Völgyesi, P., Idoeta, R., Broeckx, W., González, J. R., . . . Legarda, F. (2021). Radiological characterisation in view of nuclear reactor decommissioning: On-site benchmarking exercise of a biological shield. *Progress in Nuclear Energy. https://doi.org/10.1016/j.pnucene.2021.103740*, Volume 137, article 103740. ISSN 0149-1970.

IAEA. (1998). *Radiological Characterization of Shut Down Nuclear Reactors for Decommissioning Purposes, Technical Reports Series 389.* Vienna: IAEA.

Klein, M. (1991). *Contamination of the anti-missile slabs, Technical note.* SCK-CEN.

Klein, M. (2001). *Flux des déchets du BR3, Méthodologie de charactérisation (version 3 de l'ancien 164/99-02), 164/01-01.* Mol: SCK-CEN.

LNHB. (2018). *Nucléide - Lara, Library for gamma and alpha emissions, http://www.nucleide.org/Laraweb/index.php.* Laboratoire National Henri Bequerel.

Mandoki, R. (1994). *Caractérisation des dalles anti-missiles du BR3, Note technique RM/35/94-74.* SCK-CEN.

Mandoki, R. (1996). *Rapport de la caractérisation du bouclier biologique du BR3 (partie cylindrique), Internal report R-3107.* SCK-CEN.

Peerani, P., Boden, S., Crozet, M., & Zanovello, F. (2018). *Design of the benchmarking exercise, Deliverable 2.5, INSIDER H2020 project.* EC.

Piccini, G. (2006). *Gestion des bétons activés du BR3, Master 2 ITDD GéDéRA.* SCK-CEN.

Plateau, C. (2001). *Scabbling et découpe du béton de l'Operating Deck (11,475 m) au-dessus du Générateur de Vapeur et du Pressuriseur, Instruction de travail - démantèlement, 117/BR3/VS-419.* SCK-CEN.

Plateau, C. (2002). *Rapport de chantier 118/419-01.* SCK-CEN.

Rogiers, B., S., B., N., P., Y., D., O., S., & O., N. (2018). *Improved nulcear site characterization for waste minimization in decommissioning and dismantling operations under constraint environment. INSIDER WP3 - Sampling strategy, Report on the sampling strategy development. Deliverable D3.2 pp39.* H2020 INSIDER D3.2.

Smaizys, A. (2006). *Calculation of neutron shield tank activation level and waste management + ALARA planning (optional), internal report.* SCK-CEN.

Thierfeldt S. et al. (2012). *Berechnung von Freigrenzen und Freigabewerten für Nuklide, für die keine Werte in den IAEA-BSS vorliegen, 434.0000-101/11.007303/7918731.* Brenk Systemplanung.

Verstrepen, G. (2013). *Kernboorstalen 312-01 t.o.v. warm been - shutdown leiding: gebariteerde beton, Interne mem, 160/13-01.* SCK-CEN.

Verstrepen, G. (2016). *Cement-/betonlaag, herkomst: BR3_put NST (2 x vloer, 1 x wall), Analyserapport.* SCK-CEN.

Verstrepen, G. (2016). *Cement-/betonlaag, herkomst: BR3_put NST (2 x vloer, 1 x wall), Analyserapport, 165-16/05.* SCK-CEN.

Verstrepen, G. (2017). *Staalnamecampagne april 2017: BR3_Plan Container_Lokaal 087, Inox wand piscine, Analyserapport.* SCK-CEN.

Vincent, T. (1995). *Evaluation de l'activation des bétons du bâtiment réacteur BR3 à l'aide d'un code de transport neutronique.* DEA Radioéléments Rayonnements Radiochimie.